Continental Shelf Research 256 (2023) 104959

Contents lists available at ScienceDirect

Continental Shelf Research

journal homepage: www.elsevier.com/locate/csr

Shifts in bowhead whale distribution, behavior, and condition following rapid sea ice change in the Bering sea

John J. Citta [a,*,1], Greg A. Breed [b], Stephen R. Okkonen [c], Matthew L. Druckenmiller [d], Lori Quakenbush [a], John C. George [e], Billy Adams [e], Wieslaw Maslowski [f], Robert Osinski [g], Justin Olnes [a], Ellen V. Lea [h], Robert Suydam [e,2]

[a] Alaska Department of Fish and Game, 1300 College Road, Fairbanks, AK, 99701, USA
[b] Institute of Arctic Biology, University of Alaska Fairbanks, AK, 99775, USA
[c] Institute of Marine Science, University of Alaska Fairbanks, AK, 99775, USA
[d] National Snow and Ice Data Center, Boulder, CO, 80309, USA
[e] North Slope Borough Department of Wildlife Management, Utqiaġvik, AK, 99723, USA
[f] Department of Oceanography, Naval Postgraduate School, Monterey, CA, 93943, USA
[g] Institute of Oceanology, Polish Academy of Sciences, Powstancow Warszawy 55, 81-712, Sopot, Poland
[h] Department of Fisheries and Oceans, Inuvik, Northwest Territories, XOE 0T0, Canada

ARTICLE INFO

Keywords:
Balaena mysticetus
Sea ice
Habitat selection
Dive behavior
Diel vertical migration (DVM)

ABSTRACT

Prior to 2017, the winter (January–March) distribution of the Bering-Chukchi-Beaufort (BCB) Sea population of bowhead whales (*Balaena mysticetus*) was centered in western Bering Sea shelfwaters characterized by high concentrations of sea ice. This area was largely devoid of sea ice during the winters of 2017–19 and satellite tagging studies show that the distribution of whales shifted northwards into the Chukchi Sea during 2018 and 2019 (no winter data were available for 2017). Here, we examine how bowhead whale movements and behavior changed in response to potential ecological drivers by linking satellite tag data, collected during 2009–2019, with contemporaneous sea ice concentration data and numerical simulations of regional oceanography. We used step selection and resource selection functions to examine how whales responded to changes in sea ice concentration, modeled ocean temperature, salinity, velocity, and the local gradients in these variables. Analyses indicated that whales selected areas of intermediate ice concentrations (~65–85%) at distances ~150–250 km from the southern ice edge. Dive data suggest that, prior to the ice decline, whales spent more time near the seafloor and less time near the surface. Interestingly, we found evidence that whales may track the diel vertical migration (DVM) of krill, but only after sea ice declined. We found no change in body condition of yearling or subadult whales harvested at Utqiaġvik following 2017; however, post-weaning whales had a statistically significant decline in body condition, which could be due to changes in sea ice or could reflect negative density dependence given increases in whale abundance and density. The BCB bowhead whale population may be approaching carrying capacity and abundance is thought to have reached or surpassed what existed prior to commercial whaling. At present, overwintering in the Chukchi Sea has few negative consequences for this population and we expect over wintering within the Chukchi Sea will become more common as winter sea ice declines in the Bering Sea.

* Corresponding author.
E-mail addresses: john.citta@north-slope.org (J.J. Citta), gabreed@alaska.edu (G.A. Breed), srokkonen@alaska.edu (S.R. Okkonen), druckenmiller@colorado.edu (M.L. Druckenmiller), lori.quakenbush@alaska.gov (L. Quakenbush), craig.george@north-slope.org (J.C. George), billy.adams@north-slope.org (B. Adams), maslowsk@nps.edu (W. Maslowski), roberto@iopan.gda.pl (R. Osinski), justin.olnes@alaska.gov (J. Olnes), ellen.lea@dfo-mpo.gc.ca (E.V. Lea), robert.suydam@north-slope.org (R. Suydam).
[1] Current address: North Slope Borough Department of Wildlife Management, Utqiaġvik, Alaska, 99723 USA.
[2] Retired.

https://doi.org/10.1016/j.csr.2023.104959
Received 8 September 2022; Received in revised form 10 February 2023; Accepted 16 February 2023
Available online 18 February 2023

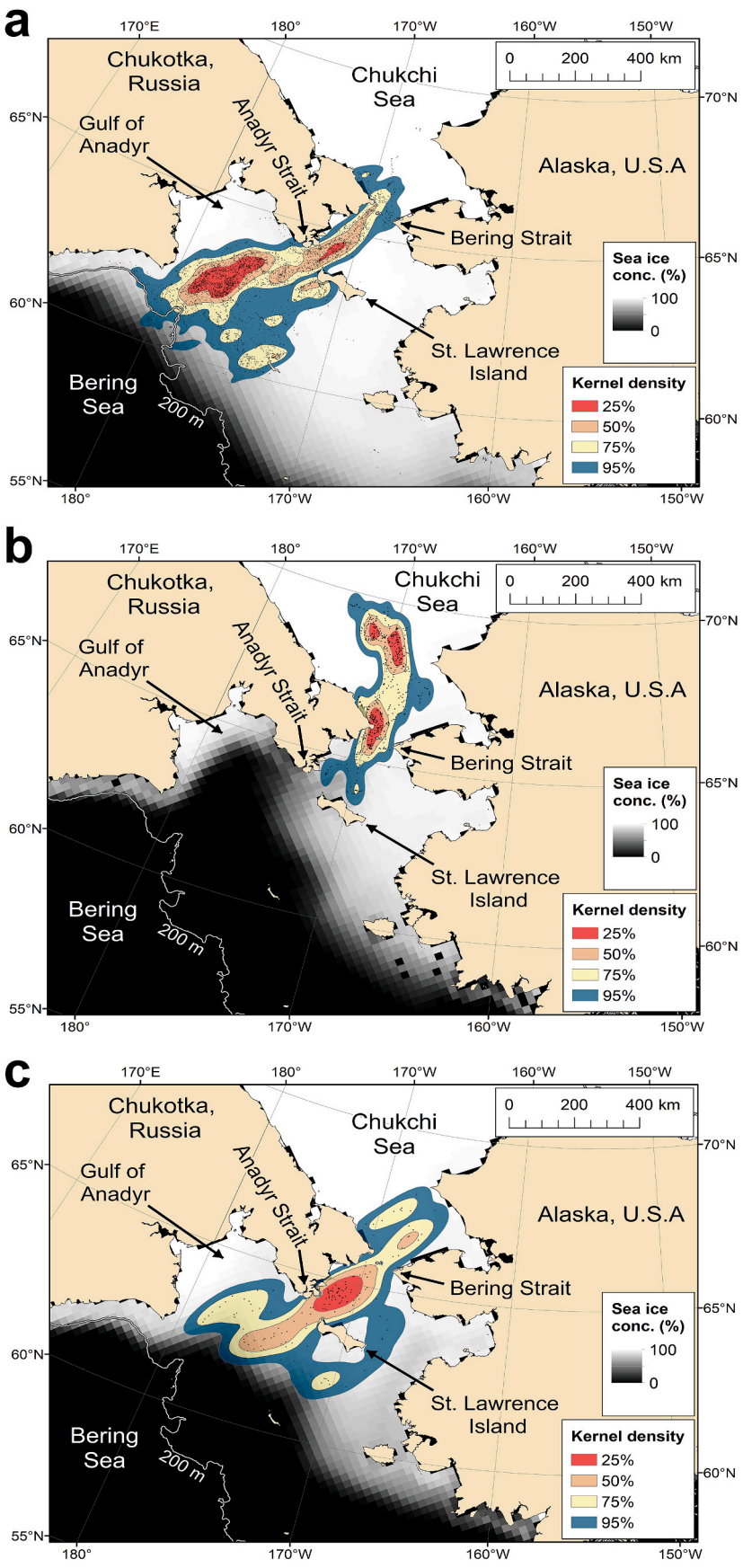

Fig. 1. (a) Density of winter (January–March) BCB bowhead transmitter locations 2009–2016 (n = 27 transmitters), (b) density of winter BCB bowhead transmitter locations 2018 (n = 3 transmitters), and (c) density of winter BCB bowhead transmitter locations in 2019 (n = 4 transmitters). Densities calculated using R package *ks* (Duong 2007; Duong and Hazelton 2005); underlying location data are shown as points within each density. In 2019, whales spent most of the winter north of St. Lawrence Island, but headed southwards when sea ice advanced in March.

1. Introduction

The northern Bering Sea is one of the most productive ocean ecosystems (e.g., Grebmeier et al., 2006) and is characterized by large seasonal changes in temperature and sea ice cover. Until recently, trends in sea ice in the northern Bering Sea were thought to be relatively resilient to climate warming and largely independent of changes documented elsewhere in the Arctic. While sea ice declined in both thickness and extent elsewhere in the Arctic (e.g., Stroeve et al., 2012), winter ice in the Bering Sea was essentially stable until well past 2010 (Moore and Laidre, 2006; Laidre et al., 2015).

Historically, Bering Sea ice typically began forming and advancing southward in November or December and decayed the following April and May (Neibauer and Schell, 1993). Ice in the Bering Sea did not extend far past the shelfbreak where storms and warmer water would break up the pack and cause it to melt. Pease (1980) described Bering Sea ice as being on a conveyor belt, forming in the north, pushed south by winds, and then melting in warmer waters near the shelfbreak. Thus, as long as winters were cold enough to freeze seawater, first-year ice would form and cover Bering Sea shelf waters.

This pattern of ice formation, transport, and melt abruptly changed during the winter of 2016/17 (Stabeno and Bell, 2019; Huntington et al., 2020) when atypically warm waters entered the Bering Sea and ice did not form south of Bering Strait until January. The winters (January–March) of 2017–2019 were subsequently characterized by delayed ice formation, reduced sea ice extent, and early retreat. Warmer, less ice-covered oceans have large and varied implications for both the physical environment and the ecosystems they support, affecting ocean circulation, nutrient cycling, primary production, and the distribution and abundance of zooplankton, fish, birds, and marine mammals (see reviews in Duffy-Anderson et al., 2019; Huntington et al., 2020).

Bowhead whales (*Balaena mysticetus*) of the Bering-Chukchi-Beaufort (BCB) population (stock) serve as important subsistence species and cultural icons to the peoples of the Alaskan and Canadian Arctic (e.g., Huntington et al., 2021). The BCB bowhead stock typically winters in the shelf waters of the northern Bering Sea, north of the shelfbreak and the southern ice margin (Ljungblad, 1986; Braham et al., 1980; Brueggeman, 1982; Moore and Reeves, 1993; Citta et al., 2012). During April, this stock begins migrating northward through Bering Strait into the Chukchi Sea, following the Alaskan coast past Point Barrow, and then proceeds eastward offshore and under the ice-covered Beaufort Sea to summering grounds in the Eastern Beaufort Sea (Moore and Reeves, 1993; Citta et al., 2015, 2021a). In late summer and autumn, whales in the Eastern Beaufort Sea begin migrating westward, following the coast back to Point Barrow, where they reach the Chukchi Sea and proceed southward as winter approaches. Sea ice typically begins to form in late November or December, and by January most whales have returned to the Bering Sea, where they again overwinter (Quakenbush et al., 2012; Citta et al., 2012, 2021a).

Telemetry data for BCB bowhead whales suggests that the winter range of bowhead whales shifted northward during the warming period that began in early 2017. During 2005–2018, a cooperative project involving native subsistence hunters, local native governments, and the Alaskan and Canadian governments, deployed 77 satellite transmitters on bowhead whales of the BCB stock, in both Alaskan and Canadian waters (see Citta et al., 2015; 2021a; Harwood et al., 2017). The historical winter (January–March) range of BCB bowhead whales was typically centered southwest of St. Lawrence Island in the Russian Bering Sea (Fig. 1, see also Braham et al., 1980; Brueggeman, 1982; Citta et al., 2021a). Warm conditions during the winters of 2017, 2018, and 2019, however, resulted in this area being almost entirely ice-free. Although no satellite transmitters were active during January–March of 2017, the first year with reduced sea ice, tagged whales wintered north of their historical range during the winters of 2018 and 2019. In March of 2019, ice reformed south of St. Lawrence Island, following two years with no sea ice, and tagged bowheads moved southwards with the ice edge towards their typical wintering area.

Why BCB bowheads shifted their winter range northward is not known. Plausible explanations include the possibility that bowhead whales prefer to remain under sea ice to avoid killer whales (*Orcinus orca*), which are known to affect the distribution of bowhead whales elsewhere in the Arctic (Matthews et al., 2020; Breed, 2021). Alternatively, bowhead whales may have shifted northwards to remain in colder water; other populations of bowhead whales have been shown to associate with water that has a relatively narrow range of surface temperatures, −0.5 to 2 °C, due to limited thermoregulatory abilities as suggested by Chambault et al. (2018). Finally, ice retreat may be correlated with other changes in the physical environment, such as changes in ocean circulation which may alter the distribution of bowhead whales by altering the availability of zooplankton prey.

Here we assess several key hypotheses explaining changes in bowhead whale wintering distributions during the warm winter climate regime that prevailed in the Bering Sea during the winters of 2017–2019, conditions that are likely to become more common. We describe the ocean environment and how it has changed, using oceanographic model data and remotely sensed sea ice data. We then use these data to fit statistical models of bowhead whale habitat selection using step selection and resource selection functions to gain insight as to what factors have caused changes in range, habitat use, and habitat selection. Additionally, we analyze dive records to assess if and how dive behavior changed, and finally, we ask if changes in the physical environment and distribution of BCB bowhead whales also resulted in detectable changes in the body condition of harvested whales.

2. Materials and methods

2.1. Datasets

2.1.1. Telemetry data

Tagging methods are described in Quakenbush et al. (2010) and Citta et al. (2015, 2018a); tagging was conducted in close collaboration with bowhead and beluga subsistence whalers who were the primary taggers. Bowhead whales were approached by small boat and satellite transmitters were attached using a 2-m or 4-m long wooden or fiberglass pole as a jab stick (Heide-Jørgensen et al., 2013). The pole system included a biopsy tip that retained a skin sample during tag deployment; this sample was used to sex whales by amplification of either zinc finger (ZFX and ZFY) genes (Morin et al., 2005) or USP9X and USP9Y genes (Bickham et al., 2011), both of which are sex determining regions within the bowhead whale genome. Whale length was estimated visually by subsistence whalers at the time of tagging. Calves less than 1 year of age and females with calves were avoided, as stipulated by research permits.

A number of different satellite transmitter models were deployed during the project and collected a range of data types. We use the word ‘tag’ to represent the transmitter and anchor hardware used to attach the tag to the whale. We deployed three tag models manufactured by Wildlife Computers of Redmond, Washington: SPOT, SPLASH, and SPLASH10. SPOT tags collected location data (i.e., latitude and longitude) only. In addition to location data, SPLASH tags also collected dive data that were summarized over 6-hr periods into histograms onboard the tag. Here we consider the Time-At-Depth (TAD) histograms, because they allow us to infer at what depths whales spend the most time. The thresholds of histogram bins (i.e., depth categories) were set prior to tag deployment; bins were set at 2, 10, 20, 30, 40, 50, 75, 100, 150, 200, 250, 300, 350, and >350 m. The final bin included all data on dives deeper than 350 m. TAD is recorded as a percentage of time within each bin over 6-hr periods, beginning daily at 0 UTC.

In addition to collecting locations and dive histogram data, SPLASH10 tags also collected more detailed information on a sample of individual dives, including the duration and maximum depth of dives, dive shape, and temperature readings paired with depth. Dive shapes include “square,” “V,” or “U” shapes; square-shaped dives are those

where >50% of the dive duration is spent near the bottom of the dive, U-shaped dives occur when 20–50% of the dive is spent at the bottom of the dive, and V-shaped dives occur when <20% of the dive is spent at the deepest depth. Square- and U-shaped dives are typically considered indicative of feeding behavior (e.g., Baumgartner and Mate 2003; Heide-Jørgensen et al., 2013).

We also included the location data from a single tag manufactured by the Sea Mammal Research Unit (SMRU) of St. Andrews, Scotland. Although this tag was capable of collecting highly resolved dive data that included paired depth-temperature and depth-salinity measurements, relatively few dives were recorded during the study period (January–March).

2.1.2. Sea ice data

Ice concentration data, used to determine daily percentages of sea ice at whale locations, were derived from satellite-based passive microwave datasets of brightness temperature. The data originate from the consecutive missions of the Special Sensor Microwave Imager (SSM/I) and Special Sensor Microwave Imager/Sounder (SSMIS) and were processed using the NASA Team algorithm (Comiso et al., 2003). Daily SSM/I and SSMIS data at 25 km × 25 km spatial resolution were accessed from the National Snow and Ice Data Center. The ice edge was defined as 15% sea ice concentration, which is the commonly used standard for passive microwave data and is the concentration at which ship-based observations begin to agree with satellite-based observations (e.g., Comiso et al., 2003; Heinrichs et al., 2006).

2.1.3. Oceanographic model data

The oceanographic model used is a version of the Regional Arctic System Model (RASM; Maslowski et al., 2012; Kinney et al., 2022), which in the full configuration includes the Los Alamos Sea Ice Model (CICE) and Parallel Ocean Program (POP), Weather Research and Forecasting Model (WRF) and Variable Infiltration Capacity (VIC) land hydrology model coupled using the Community Earth System Model (CESM) flux coupler (CPL7). We used a subset of the RASM model, where the atmospheric and land models are replaced with prescribed realistic atmospheric reanalyzed data from the Common Ocean Reference Experiment version 2 (CORE2) 1948–2009 reanalysis. This approach allows direct comparison of model results with observations as well as investigation of the importance of mesoscale ocean and sea ice processes and interactions among them.

The ocean and sea ice models are configured on the same rotated spherical 1/12-degree and 45-level grid, with eight depth levels in the upper 53 m and 15 levels in the upper 220 m. The model domain covers the entire Northern Hemisphere marine cryosphere and extends south to ~30° N latitude in the North Pacific and ~40–45° N latitude in the North Atlantic. The high spatial resolution and the large domain allow simulation of most of the important processes in the Arctic Ocean, including those over the shelves and in the upper ocean of the deep basin, and realistic exchanges between the Bering and Chukchi seas.

Temperatures and salinities were extracted from the grid for use as covariates for the habitat selection models (see Sections 2.2.2 and 2.2.3) using IDL (https://www.l3harrisgeospatial.com/Software-Technology/IDL). Because this stock of whales is known to predominantly feed near the seafloor in winter (Citta et al., 2012, 2021a), we extracted bottom values. The depth of Bering and Chukchi shelves range from ~50 m to 200 m. For the 50–200 depth range, bottom temperatures and salinities were extracted from model depth bins 8 (42.08–52.67 m) through 15 (181.49–220.84 m).

2.1.4. Body condition data

An index of body condition (BCI) was calculated using length and girth measurements from whales harvested at Utqiaġvik during 1993–2018 (see George et al., 2015). Axillary and umbilical girth were averaged and divided by body length. Following George et al. (2015), we defined four age classes when assessing changes in BCI, based on the length of the longest baleen plate: yearlings (age 1.0–1.5 yrs) were classified by baleen length between 50 and 90 cm; postweaning (age ~2–5 yrs) were classified by baleen length between 90 and 140 cm, subadults (age ~6–20) were classified by baleen length between 140 and 250 cm, and adults (age ~20+ yrs) were classified by baleen length >250 cm (Lubetkin et al., 2008, 2012).

2.2. Statistical analyses

2.2.1. Location processing

Prior to performing analyses of habitat selection (described in sections 2.2.2 and 2.2.3) we estimated locations from each animal's raw Argos relocations using the Continuous-Time Correlated Random Walk (CTCRW) model developed by Johnson et al. (2008) and implemented in the R package *crawl*, version 2.0 (Johnson and London, 2018), in R (R Core Team, 2022). Because the CTCRW algorithm performs poorly when Argos error greatly exceeds measured values and model priors, Johnson et al. (2008) recommended pre-filtering Argos locations to remove locations with extreme error. Thus, we passed the raw location data through the sdafilter in R package *argosfilter* (Freitas et al., 2008; Freitas, 2012). We set the velocity threshold to 4 m/s, which is approximately twice the maximum known velocity of bowhead whales (Zeh et al., 1993). We also removed locations that formed angles <45° when they were farther than 15 km from the previous location. We used a distance threshold of 15 km based on Vincent et al. (2002), who found that 95% of low-quality locations (location class = B) were within 15 km of the true location.

The CTCRW model assumes movement is a velocity process with two parameters, β, the autocorrelation in velocity and σ, the variation in velocity. Location error was assumed to be normally distributed with a mean of 0 and a standard deviation equal to that declared by CLS for GPS locations, and location classes 3, 2, and 1. We treated the standard deviations for the remaining three location classes (0, A, and B) as parameters which were estimated and fitted using log normal distributions with semi-informative priors. Locations with classes 0, A, and B should have more error than those with a class of 1 (SD = 1500 m). Hence, we imposed a lower bound of 1500 m on half normal distributions. Using data from Vincent et al. (2002), our priors had a mean error 1500 m and a standard deviation of 5000 m for location classes 0 and A, and 7500 m for location quality score B. We set Laplace priors (double exponential) for the velocity parameters β and σ, with a mean of 3 and a variance of 0.5 on a natural log scale, which is approximately the value of β and σ empirically observed for bowhead whales. The CTCRW will estimate an animal's location during periods for which no Argos relocations were collected. Such gaps occasionally occur due to storms, heavy ice, suboptimal tag placement, or when batteries are low. However, we only use locations from the CTCRW model when actual Argos locations were collected within 24 h of the estimated location; data with longer gaps were not included in this analysis. These specifications for the CTCRW model are similar to those used in Citta et al. (2018b) with the exception that here we estimated locations with 6-hr intervals to align with TAD histograms so the histograms could be mapped, whereas Citta et al. (2018b) estimated locations at 24-hr intervals.

2.2.2. Step selection analysis

We implemented a step-selection function (SSF) to evaluate how sea ice and other environmental covariates affect whale movement from one step to the next (i.e., one location to the next). For each real location in an animal's track, a set of control locations available at the next time step (t+1) were drawn, conditional on the animal's position at time t. Control locations are typically generated by drawing steps from fitted probability distributions describing the turning angle and step length from a fitted CRW or from the empirical step length and turning angle distributions. Depending upon the application, between 1 and 20 available steps are drawn from each real location at time t, and these potential steps are compared to the actual relocation observed at time

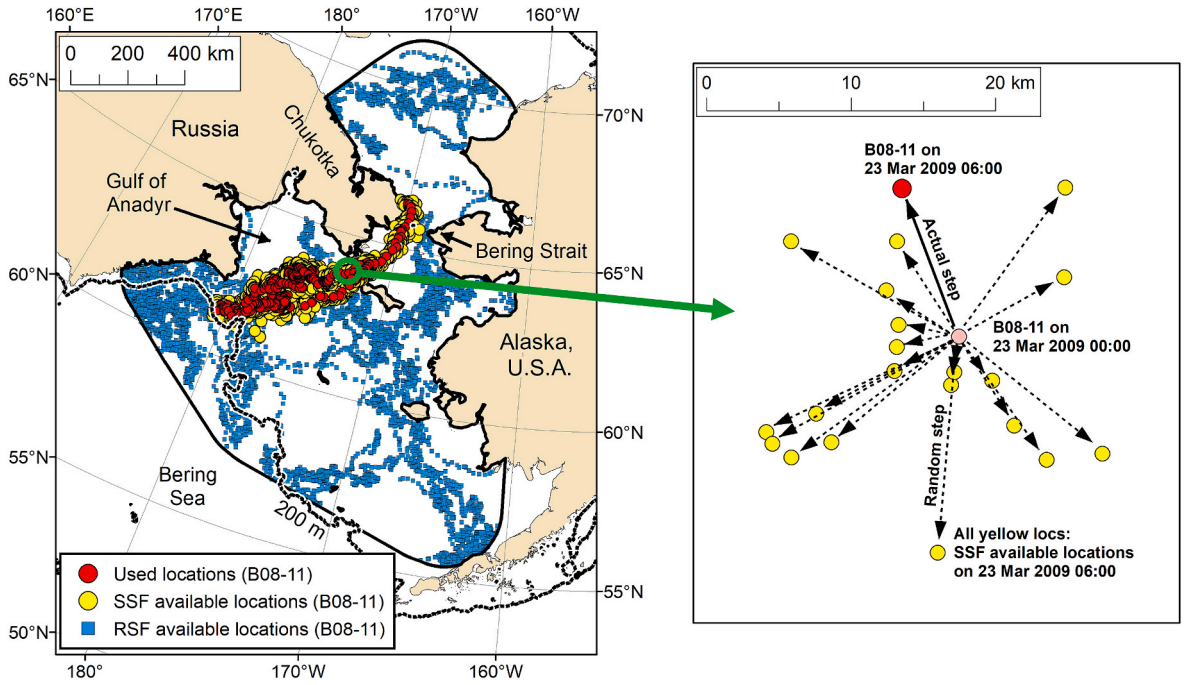

Fig. 2. Example of used and available locations for one whale, B08-11. On the left, the set of used locations (red circles), available locations for Step Selection Functions (SSF; yellow circles), and available locations for Resource Selection Functions (RSF; blue squares) are shown. On the right, is one example for the step length and direction of a used track (pink to red) and the corresponding random steps for habitat comparisons. Note that the SSF compares selected locations at a small scale and the RSF compares selected locations across the winter range.

t+1 using a conditional logistic regression (Fortin et al., 2005; Thurfjell et al., 2014; Avgar et al., 2015). For SSFs, comparisons are conditioned on the starting location and restricted to the relative differences between the selected location and that locations available, with each step compared within its own conditional cluster.

For this analysis we generated 20 matched control (i.e., available) locations by drawing steps from empirical step length and turn angle distributions (Thurfjell et al., 2014). Any steps that fell on land were redrawn so that all control locations occurred in the ocean. After matched control cases were generated, we extracted environmental covariate data at each real and control location from covariate datasets. Candidate models included three key sea ice covariates: sea ice concentration, distance to sea ice edge, and an indicator variable (is_{ice}: 0 when whales were in south of the ice edge in open water, and 1 when they were north of the ice edge) because we expected any effect of distance to ice edge to differ depending upon whether individuals were in front of or behind the edge (e.g., Breed et al., 2018; Matthews et al., 2020). The position of the sea ice edge was dynamic and defined as the 15% ice concentration isopleth. Oceanographic covariates included water depth, bottom temperature, velocity, and bottom salinity as well as the spatial gradients of each, which may be proxies for oceanographic frontal features with the potential to aggregate prey. Because sea ice concentration is a proportion, it was logit transformed. Similarly, because distances to ice edge and depths are continuous and positive they were log transformed. These transformations improved model fit and convergence.

The matched control cases were compared to the steps animals selected with a series of candidate conditional logistic regression models using the clogit function in the R package *survival* (Therneau, 2022). The conditional logistic regression took the general form:

$$\text{logit}(\eta_{i,j}) = \beta_1 x_{1,i,j} + \beta_2 x_{2,i,j} \cdots \beta_p x_{p,i,j} + \nu_j \quad (1)$$

$$use_{i,j} \sim \text{Binomial}(\eta_{i,j},\ 1) \quad (2)$$

where $use_{i,j}$ indicates whether a location was a true relocation (1) or a matched case-control location (0), i indexes the specific relocation, and j indexes the individual whale. β's are the linear parameters on the environmental covariates (x's) and ν_j was included as an individual random effect for jth bowhead whale. Conditional logistic regressions are fit using Cox proportional hazard model to estimate relative differences within the set of matched cases (clusters); consequently, they have no intercept (β_0). Finally, step length was included as a nuisance parameter to control bias in parameter estimates, as locations closer to the start of the step are more likely to be selected (Forester et al., 2009).

2.2.3. Resource selection analysis

To understand how the sea ice and oceanographic conditions covariates affected the probability bowhead whales used a particular habitat, we also fit resource selection functions (RSFs). In an RSF, the case controls are drawn from a much larger area and comparisons between used and control locations are not matched to individual steps. Consequently, an RSF provides inference about differences in occupied versus unoccupied habitat across an animal's range.

We used generalized linear mixed models (GLMMs) fit with the glmer function in R package *lme4* (Bates et al., 2015) with a logit link and binomial errors (i.e., a logistic regression; Manly et al., 2002; Breed et al., 2018). The general form of the RSF models used here was essentially identical to Eqs. (1) and (2) as described in the SSF section, except that they were fit as an ordinary logistic regression and thus include an intercept (β_0). The response variable was *use*, which indicated whether the location was associated with the control location (0) or a real location (1) and were related to the series of environmental covariates (x's) via estimated parameters (β's).

2.2.4. Control location generation

Control locations for RSF models were generated by simulating psuedotracks – simulated movement pathways generated using the fitted movement parameters from package *crawl* during initial Argos location processing (e.g., Citta et al., 2018a; Breed et al., 2018). For each tracked bowhead whale, 20 simulated tracks were generated, with locations every 6 h, such that each simulated track had exactly the same number of locations and the same location timestamps as the real track.

The bounds for pseudotracks were defined as the range of actual bowhead locations, plus a 200 km buffer (Fig. 2). Each of the 20 psuedotracks originated from a random location within the 200 km buffer area, with landmasses treated as reflective boundaries so that simulated movements could not cross land-sea boundaries. When generating pseudotracks, we used the actual step length of the whale, combined with a random draw from the actual distribution of bowhead turn angles. This method ensured pseudotracks were structurally similar (i.e., in terms of vector components) to their paired real tracks, but without the influence of habitat.

2.2.5. Monte Carlo robust RSF Parameters and uncertainties

In a typical RSF, fit via logistic regression, the set of real cases (i.e., the relocation data from the tracked animals) are matched and compared to control locations that are randomly selected from an animal's potentially useable habitat (Manly et al., 2002). In most RSF analyses, including this one, there is no clear way to delineate the potential habitat region from which control locations might reasonably be selected. One way to resolve this is to simulate pathways using movement parameters derived from observed data, which, as described earlier, was the solution we chose.

However, this creates a new problem. Both the real and control locations are autocorrelated, which will bias the estimated parameter variances of the logistic regression downward such that the uncertainty regions are unrealistically small (Fieberg et al., 2010), and commensurately biasing significance tests. The actual parameter estimates, however, should be unbiased (Schabenberger and Gotway, 2005). Thus, for each of the 20 CRW pseudotracks, the RSF was refit using each of the 20 sets of control cases (i.e., the individual pseudo-tracks) separately. This produced a population of 20 parameter estimates, each associated with a different control psuedotrack. We discarded the estimated variances from each of 20 logistic regression model fits, which are biased due to autocorrelation, but retained the parameter estimates. Variances were instead calculated from the population of parameter estimates of the 20 separate model fits, which yields a reasonably unbiased estimate of parameter uncertainty from which 95% confidence intervals were then calculated. This approach assumes the parameter estimates are normally distributed, which appeared to be the case upon inspection of the estimates, and that each of the 20 Monte Carlo simulated trackways were independent of each other. We then proceeded with normal parametric inference. For each parameter, we tested the null hypothesis that regression coefficients equaled zero; standard errors and p-values were obtained by assuming mean regression coefficients were distributed normally with standard deviation as obtained from the 20 Monte Carlo fits of the logistic regression. This allowed us to assess the probability that the uncertainty region around each parameter estimate contained 0 (i.e., the p-value). This "robust approach" has been used for a variety of RSF analyses (e.g., Breed et al., 2018; Citta et al., 2018a; Cameron et al., 2020). The robust approach was only required for RSF models; the nature of the conditional logistic regression fit via Cox proportional hazard in the SSF does not produce biased parameter uncertainty regions after controlling for step length (Forester et al., 2009).

2.2.6. Model selection and covariates

Competing SSF models were selected using AICc (Burnham and Anderson, 2002). However, likelihood-based model-selection procedures, such as AIC, are not valid when using Monte Carlo methods for estimating parameter means and standard errors, as we did for fitting RSF models. Hence, we used backwards stepwise selection to remove non-significant parameters one-at-a-time for RSF models.

Covariates for both SSF and RSF candidate models included ice concentration, ice concentration squared, distance to the ice edge, and a binary variable that indicated if ice was present. From the oceanographic model (RASM) we included seafloor temperature, seafloor salinity, velocity, and the gradient magnitudes, G, of seafloor temperature (°C/km) and salinity (psu/km).

$$G = \sqrt{\left(\frac{\partial \varphi}{\partial x}\right)^2 + \left(\frac{\partial \varphi}{\partial y}\right)^2},$$

in which φ is the oceanographic property of interest (temperature or salinity) and the derivatives are approximated as central differences.

After arriving at our final model, we proceeded to test if selection parameters differed before and after 2017 (period effects), when sea ice conditions suddenly changed, by sequentially adding an interaction term for the period effect to each term of the best fitting model. If selection for sea ice conditions changed after ice became degraded, the addition of interaction terms for period should improve fit as assessed via AICc for SSF models. For RSF models, changes in parameter values could be assessed by adding the period effect, which created two parameter estimates (one in each period). We could then assess if the parameters were significantly different from each other using a two-sample t-test from the sample of 20 Monte Carlo model fits.

2.2.7. Modeling dive data

Using TAD data from 23 whales, we calculated four TAD variables: (1) the proportion of time whales spent at the surface (i.e., within 2 m), (2) the proportion of time spent near the seafloor, (3) the probability whales visited the seafloor during a 6-hr histogram period, and (4) the depth bin in which the most time was spent (i.e., target depth). The proportion of time spent at the seafloor was equal to the TAD value in the depth bin that overlapped bathymetric depth; bathymetric depth was linked to TAD histograms by matching timestamps from the TAD histograms with those from the CRW location model for each whale. Bathymetric depth was taken from the ARDEM v2.0 grid, available through the Alaska Ocean Observing System (Danielson et al., 2015; available at: www.aoos.org), using ArcGIS 10.8.2 (https://www.esri.com/).

We fit each TAD variable to a linear mixed effects model using package *nlme* (Pinheiro et al., 2022) in R. Models included individual as a random intercept and accounted for repeated measurements as an autoregressive process of order 1 on a continuous time-scale (i.e., corCAR1). Covariates included *ice period* (i.e., before and after the 2017 sea ice decline), *sex*, and *age*. The proportions of time spent near the surface and seafloor, and target depths generally did not have values close to 1 or 0 and confidence limits did not approach those boundaries, hence these variables were modeled with normal distribution and no transformations. However, the probability of visiting the seafloor approached 1; therefore, we logit transformed this variable prior to analysis. All models were ranked using AIC.

For a smaller sample of whales, those with SPLASH10 tags (n = 7), we also examined statistics from a sample of individual dives. Statistics included: (1) dive duration, (2) dive depth, (3) distance from the seafloor, and the proportions of (4) square-, (5) U-, and (6) V-shaped dives. As with the TAD variables, we modeled statistics 1–3 with linear mixed effects models using package *nlme* (Pinheiro et al., 2022). As before, models included whales as random intercepts and models included an autoregressive process of order 1 on a continuous timescale (corCAR1). Covariates included *ice period* (i.e., before and after 2017), *sex*, and *age*. Because individual dives can only have a single shape, we modeled the proportions (variables 5–6) using generalized linear mixed models in R package *MASS* (Venables and Ripley, 2002) with a logit link (i.e., logistic regression). Again, individuals were modeled as random intercepts with a corCAR1 autoregressive process and covariates included *ice period*, *sex*, and *age*. Models were ranked using AICc (Burnham and Anderson, 2002).

Dive depth of bowhead whales is sometimes known to track the diel vertical migration (DVM) of zooplankton (e.g., Fortune et al., 2020, 2021). The TAD data are not well suited for identifying such patterns because the 6-hr summary periods cover periods of both daylight and darkness. However, we can examine the effect of time-of-day on dive depth using the sample of individual dives from the SPLASH10 tags. To

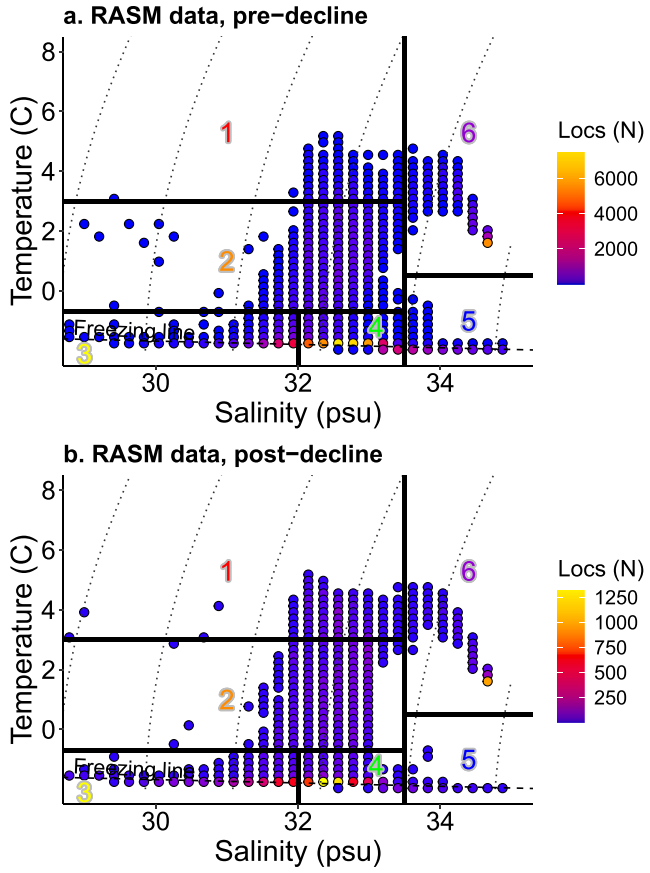

Fig. 3. Temperature and salinity plots for the RSF available set of locations (a) before ice decline and (b) after ice decline. Temperature and salinity are taken from the seafloor on the shelf (<200 m); off the shelf, values are taken at 200 m as bowhead whales typically do not dive deeper in winter. This T-S plot is a general description of what water masses are available within the sample range of bowhead whales. Numbers 1–6 correspond to ad hoc definitions of water masses, also shown in Fig. 5.

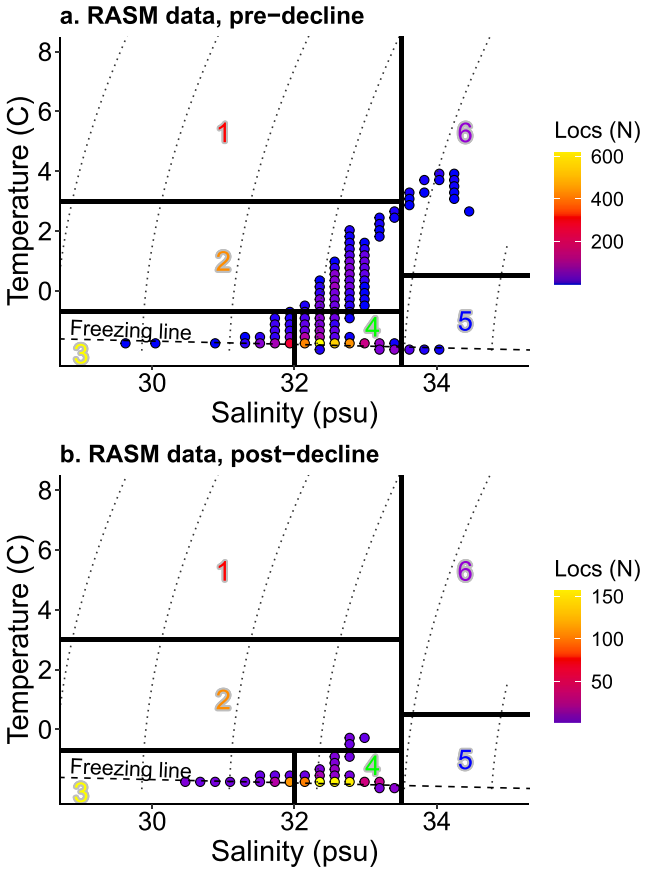

Fig. 4. Temperature and salinity plots for the used set of locations (i.e., values at whale locations) (a) before ice decline and (b) after ice decline. Temperature and salinity are taken from the seafloor on the shelf (<200 m); off the shelf, values are taken at 200 m as bowhead whales typically do not dive deeper in winter. Numbers 1–6 correspond to ad hoc definitions of water masses, also shown in Fig. 5.

do this, we used generalized additive models (GAMs; Wood, 2011) to explore the possibility that whales track the DVM of zooplankton in winter. We restricted our examination to square- and U-shaped dives that were ≥1 min in duration, as these are expected to be most indicative of feeding behavior. Times were converted to the solar hour at 170 West longitude, and dive depth was modeled as a smoothed function of *solar hour* and additive functions of *ice period* (again, before and after 2017). We used default settings (thin plate regression splines; Wood, 2003) for smoothing by solar hour and Gaussian errors. As before, models included random intercepts for individual whales and a corCAR1 autoregressive process. Data were insufficient to stratify by sex or age, so these effects were not included.

2.2.8. Modeling body condition

Bowhead whales are harvested at Utqiaġvik in spring and autumn. Because we wanted to isolate changes in body condition that occurred over winter from overall trends in body condition, we initially hoped to examine the annual difference between spring body condition versus the previous fall. However, data were insufficient to calculate annual differences; because of this we settled on fitting the spring measurements as an intercept adjustment. This allowed us to use simple linear models with normal errors to estimate how body condition has changed by ice period. Each age class was modeled separately; covariates included *season* and *ice period* (before and after 2017) as intercept adjustments and the linear trend of year. Models were ranked using AICc (Burnham and Anderson, 2002).

3. Results

Telemetry data were collected from 34 bowhead whales, 27 prior to the sea ice decline in 2017 and 7 after the 2017 decline. The sample was dominated by immature whales (i.e., <13 m); 74% (20 of 27) prior to 2017 and 86% (6 of 7) after 2017 were immature. The sex ratio was skewed towards males prior to 2017, with 70% (14 of 20) males. Prior to 2017, the sex of 7 whales, were unknown. After 2017, 57% (4 of 7) whales were male.

3.1. Sea ice and oceanographic model data at sampling locations

Sea ice concentration taken from the sample of available locations (from the pseudotracks generated for the RSF analysis) shows that the average concentration of sea ice during January–March declined from 58% (SD = 39) to 37% (SD = 40) after 2017. In contrast, average sea ice concentration at used locations (i.e., actual whale locations) remained relatively constant, declining from 79% (SD = 16) to 74% (SD = 16) after 2017. Prior to sea ice decline, only 4 of 5688 used locations (<0.01%) were south of the southern ice margin in open water, all occurring in 2010. All four locations were for whale B09-09, a mature whale of unknown sex.

Oceanographic model data taken from the sample of available pseudotrack locations show that a similar range in temperatures and salinities existed before and after the sea ice decline in 2017 (Fig. 3), although the distribution of those waters shifted (see below). In both

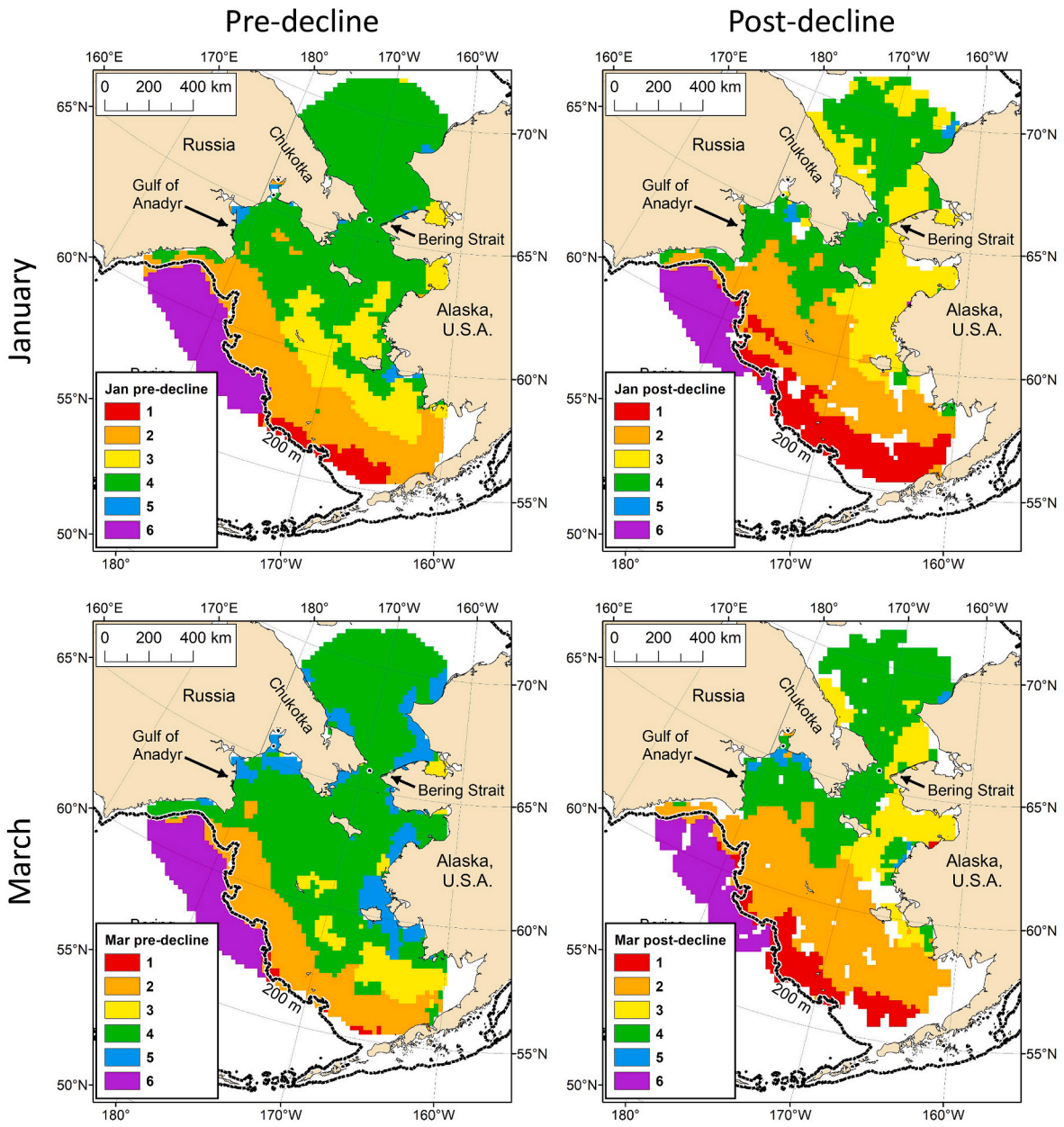

Fig. 5. Spatial distributions of ad hoc water masses shown in Figs. 3 and 4. Most common water mass is shown for pre- and post-declines in sea ice (left vs. right columns), and early and late winter (January and March). Values are taken from the set of available RSF locations. Gaps in the post-decline period are due to having fewer whales and fewer available locations.

periods, used locations (i.e., the actual locations of whales) were clustered in waters ranging from 32 to 33 psu and <-1 °C (Fig. 4). After 2017, whales were never located in water warmer than 0 °C (Fig. 4), largely because after 2017, whales were located farther north of the shelfbreak and away from the influence of warmer, upwelled deep water. To illustrate the spatial distribution of temperature (T) and salinity (S), we split T-S space into six ad hoc water masses (see numbers in Figs. 3–5). Locations associated with warmer bottom temperatures (~>0 °C) were generally located near the shelfbreak (water masses #1 and #2) or in deep basin waters (water mass #6), which cool more slowly than shallow shelf waters (Fig. 5).

3.2. Step and resource selection functions

The best fitting SSF and RSF models were the same when using 6- or 24-hr relocation data. Because both data sets resulted in the same models being selected, we report only the results of the models fit to the 24-hr data.

3.2.1. Step Selection Functions

In the best fitting SSF model, nearly all of the variance was explained by sea ice covariates, and the second ranked model included ice concentration and ice concentration squared, distance to the ice edge and distance to the edge squared. This model suggested that selection was essentially zero for open water and initially increased with ice concentration and distance to the ice edge, after which selection declined as ice concentration and distance to the edge increased. Whales with transmitters were most likely to turn in the direction of intermediate sea ice concentrations (~65%) and tended to remain ~160 km north of the ice edge (Fig. 6, left). The inclusion of period effects, to determine if selection may have changed following the change in ice conditions in 2017, did not improve fit. The best model including period effects was

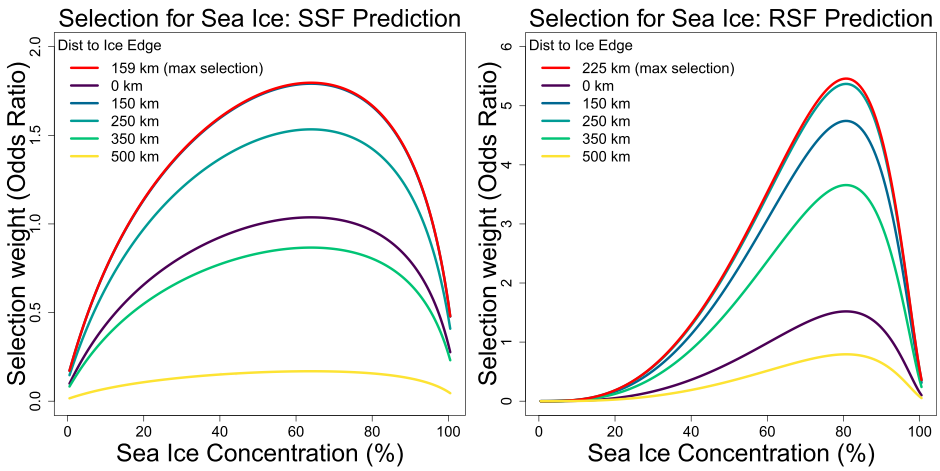

Fig. 6. Odds ratios of selection for sea ice concentration (%) across a range of distances from the southern ice margin (km) for SSF (left) and RSF (right) models of BCB bowhead winter habitat selection.

40 AICc units from the best approximating model, indicating that selection at the scale of 24-hr steps did not change by period. In addition, a small amount of variation was explained by the gradient in bottom temperature, which reduced AIC by 5.67 compared to the ice-only model (Table 2). Whales tended to select steps into habitats that had higher bottom temperature gradients (Table 3); this effect did not change between periods. No other oceanographic covariates improved model fit (Table 2).

3.2.2. Resource selection functions

The best fitting RSF model also included ice concentration and ice concentration squared, distance to the ice edge and distance to the edge squared. However, in addition to these ice covariates, seafloor temperature gradient (gradT), seafloor velocity (V) and seafloor salinity gradient (gradS) also improved the fit of the RSF (Table 4). As with the SSF model, the RSF model indicated that whales tended to avoid both areas of open water and heavy sea ice (Fig. 6, right); however, the RSF model indicated whales selected regions associated with higher concentrations of sea ice than the SSF model indicated, with a peak at ~85%. Furthermore, whales selected regions farther north, behind the ice edge, with selection peaking at ~225 km north of the ice edge. Additionally, whales selected regions with elevated current velocity, lower salinity gradients, and higher temperature gradients (Table 4).

Period effects were statistically significant ($p < 0.05$) for sea ice concentration and sea ice concentration squared, distance to the ice edge and distance to the edge squared. After ice conditions changed in 2017, selection for the intermediate sea ice concentration intensified, along with selection for intermediate distance to the ice edge. This intensification can be observed in the odds ratios for selection (Fig. 7). For example, prior to 2017, whales were ~3 times more likely to select areas with 85% sea ice concentration than areas with only 10% concentration. After 2017, whales were ~5 times more likely to select areas with 85% sea ice concentration than areas with only 10% concentration.

There were no period effects on selection for bottom velocity. However, selection for gradients in both bottom temperature and bottom salinity changed by period. Before 2017, these effects were strong in their respective direction (i.e., selection for stronger gradients in temperature and against stronger gradients in salinity). After 2017, during the warmer, ice degraded period, selection effects for both temperature and salinity gradients were not different from zero, indicating they became non-significant factors in habitat use patterns after 2017. These patterns are visually apparent; whales were co-located with areas characterized by elevated temperature gradients, low salinity gradients, and elevated seafloor velocities prior to sea ice declines and only co-located with higher seafloor velocities after sea ice declines (Fig. 8).

3.3. Dive data

3.3.1. Time-At-Depth (TAD) histograms

A total of 2052 TAD histograms were collected during January–March, 1685 prior to the ice decline in 2017 and 367 afterwards. Prior to the sea ice decline, TAD histograms were associated with a greater average depth (84.9 m versus 49.1 m; Table 5), because whales frequented areas closer to the shelfbreak where waters are deeper. However, these differences were not consistent nor statistically significant ($p = 0.12$).

The best approximating model for proportion of time spent within 2 m of the surface included the variable *ice period*, only. This model suggested that whales spent less time near the surface prior to the sea ice decline ($\bar{x} = 31\%$, 95% CI = 26–35%; Table TAD) than after the sea ice decline ($\bar{x} = 50\%$ of 6-hr intervals; 95% CI = 42–59%). The only other model within 2 AICc of the best approximating model included the variable *sex* (Δ AICc = 1.9). However, it was whales with unknown sex that differed; there were no detectable differences between whales known to be male or female ($p = 0.46$).

The best approximating model for proportion of time spent at the seafloor included the variables *ice period* and *sex*. The model suggested that whales spent a larger proportion of time near the seafloor prior to the ice decline ($\bar{x} = 33\%$ of 6-hr intervals; 95% CI = 26–35%) than after the decline ($\bar{x} = 17\%$ of 6-hr intervals; 95% CI = 05–28%). Again, it was whales with unknown sex that differed; there were no detectable differences between whales known to be male or female. The only other model within 2 AICc units of the best approximating model also included the variable *age* (Δ AICc = 0.8). This model suggested mature whales spent approximately 10% less time at the seafloor than immature whales; however, the coefficient overlapped 0 ($\bar{x}$ = -10.2% of 6-hr intervals; 95% CI = −23.3–2.3%) and was non-signification once REML was used to fit the covariance structure ($p = 0.12$).

The best approximating model for target depth (i.e., the depth bin in which whales spent the most time) included the variables *ice period* and *sex*. This model suggested that whales targeted deeper depths prior to the sea ice decline ($\bar{x}$ = 59.8 m; 95% CI = 50.9–68.6 m) than after decline in sea ice ($\bar{x} = 22.0$ m, 95% CI = 4.6–39.3 m; Table 5). Yet again, it was whales with unknown sex that differed; there were no detectable differences between whales known to be male or female. No other models were within 2 AICc units of the best approximating model.

3.3.2. Sampled dives

Seven whales had SPLASH10 tags capable of collecting statistics from individual dives (Table 1). Prior to the sea ice decline, 405 dives were sampled from three whales (Table 6). After the decline, 1454 dives

Table 1
Characteristics of 34 bowhead whales used in analyses of movement and dive behavior during winter (January–March). Lengths are estimated visually and are approximate; "mature" whales are ≥13 m in length (Koski et al., 2013). M = male, F = female, and Unk = unknown.

ID	Tagging location	Starting date	Ending date	Tag type	Length (m)<	Age	Sex	TAD histograms	Samples of individual dives	Ice period
B08-01	Tuktoyaktuk, NT	1-Jan-2009	29-Mar-2009	SPLASH	10.7	Immature	Female	Yes	No	Pre-decline
B08-06	Utqiaġvik, AK	1-Jan-2009	12-Mar-2009	SPLASH	10.0	Immature	Unk	Yes	No	Pre-decline
B08-07	Utqiaġvik, AK	1-Jan-2009	31-Mar-2009	SPLASH	10.0	Immature	Male	Yes	No	Pre-decline
B08-08	Utqiaġvik, AK	1-Jan-2009	31-Mar-2009	SPLASH	10.0	Immature	Unk	Yes	No	Pre-decline
B08-09	Utqiaġvik, AK	6-Jan-2009	31-Mar-2009	SPOT	9.1	Immature	Male	No	No	Pre-decline
B08-10	Utqiaġvik, AK	1-Jan-2009	31-Mar-2009	SPOT	10.0	Immature	Male	No	No	Pre-decline
B08-11	Utqiaġvik, AK	1-Jan-2009	31-Mar-2009	SPOT	10.0	Immature	Male	No	No	Pre-decline
B08-12	Utqiaġvik, AK	1-Jan-2009	31-Mar-2009	SPOT	9.1	Immature	Male	No	No	Pre-decline
B08-13	Utqiaġvik, AK	1-Jan-2009	12-Mar-2009	SPLASH	10.0	Immature	Unk	Yes	No	Pre-decline
B08-14	Utqiaġvik, AK	1-Jan-2009	31-Mar-2009	SPOT	13.7	Mature	Male	No	No	Pre-decline
B09-02	Utqiaġvik, AK	4-Jan-2010	30-Jan-2010	SPLASH	13.7	Mature	Unk	Yes	No	Pre-decline
B09-04	Tuktoyaktuk, NT	1-Jan-2010	31-Mar-2010	SPLASH	10.0	Immature	Male	Yes	No	Pre-decline
B09-05	Tuktoyaktuk, NT	1-Jan-2010	31-Mar-2010	SPLASH	10.0	Immature	Male	Yes	No	Pre-decline
B09-08	Utqiaġvik, AK	11-Jan-2010	17-Mar-2010	SPOT	13.7	Mature	Male	No	No	Pre-decline
B09-09	Utqiaġvik, AK	1-Jan-2010	31-Mar-2010	SPLASH	13.4	Mature	Unk	Yes	No	Pre-decline
B09-13	Utqiaġvik, AK	1-Jan-2010	31-Mar-2010	SPLASH	8.2	Immature	Female	Yes	No	Pre-decline
B09-15	Utqiaġvik, AK	1-Jan-2010	31-Mar-2010	SPLASH	11.3	Immature	Female	Yes	No	Pre-decline
B09-16	Utqiaġvik, AK	1-Jan-2010	31-Mar-2010	SPOT	13.1	Mature	Male	No	No	Pre-decline
B10-08	Tuktoyaktuk, NT	29-Jan-2011	30-Mar-2011	SPLASH	10.7	Immature	Unk	Yes	No	Pre-decline
B10-09	Herschel Is., YT	2-Jan-2011	8-Mar-2011	SPOT	9.1	Immature	Female	No	No	Pre-decline
B10-11	Tuktoyaktuk, NT	1-Jan-2011	11-Feb-2011	SPLASH	12.2	Immature	Male	Yes	No	Pre-decline
B10-12	Tuktoyaktuk, NT	3-Jan-2011	12-Feb-2011	SPLASH	11.4	Immature	Female	Yes	No	Pre-decline
B10-14	Tuktoyaktuk, NT	1-Jan-2011	31-Mar-2011	SPLASH	12.2	Immature	Male	Yes	No	Pre-decline
B10-15	Tuktoyaktuk, NT	1-Jan-2011	29-Mar-2011	SPLASH	12.2	Immature	Female	Yes	No	Pre-decline
B12-03	Utqiaġvik, AK	1-Jan-2013	6-Feb-2013	Splash10	13.7	Mature	Male	Yes	Yes	Pre-decline
B14-01	Tuktoyaktuk, NT	1-Jan-2015	27-Feb-2015	Splash10	9.1	Immature	Unk	Yes	Yes	Pre-decline
B15-01	Utqiaġvik, AK	3-Mar-2016	31-Mar-2016	Splash10	13.7	Mature	Male	Yes	Yes	Pre-decline
B17-01	Tuktoyaktuk, NT	1-Jan-2018	31-Mar-2018	Splash10	7.6	Immature	Male	Yes	Yes	Post-decline
B17-02	Tuktoyaktuk, NT	1-Jan-2018	31-Mar-2018	Splash10	10.7	Immature	Female	Yes	Yes	Post-decline
B17-03	Tuktoyaktuk, NT	14-Feb-2018	28-Mar-2019	Splash10	10.7	Immature	Female	Yes	Yes	Post-decline
B18-02	Utqiaġvik, AK	4-Jan-2019	24-Jan-2019	Splash10	10.7	Immature	Male	Yes	Yes	Post-decline
B18-03	Utqiaġvik, AK	1-Jan-2019	31-Mar-2019	Splash10	7.6	Immature	Male	Yes	Yes	Post-decline
B18-04	Utqiaġvik, AK	1-Jan-2019	2-Feb-2019	Splash10	13.7	Mature	Female	Yes	Yes	Post-decline
B18-09	Utqiaġvik, AK	28-Feb-2019	29-Mar-2019	CTD	12.2	Immature	Male	No	Yes	Post-decline

Table 2
Top 12 models of selection from the step-selection function (SSF) analysis. Abbreviations of covariates: ice = sea ice concentration; d_edge = distance to the southern ice margin in km; T = seafloor temperature (C°); S = seafloor salinity; V = seafloor current velocity (cm/s); "grad" denotes the gradient in T, S, or V (see text for how this is calculated); "full ice" denotes that all ice covariates are included, specifically, [full ice] = ice + ice^2 + d_edge + d_edge^2. All SSF models also include step length as a covariate to control for bias in parameter estimates (Forester et al., 2009).

Model	df	AIC	ΔAIC
[full ice] + gradT	6	10874.4	–
[full ice]	5	10880.07	5.67
[full ice] + gradS	6	10880.71	6.31
[full ice] + V	6	10881.23	6.83
[full ice] + gradV	6	10881.52	7.12
[full ice] + S	6	10881.77	7.37
[full ice] + temp + temp^2	7	10883.24	8.84
d_edge + d_edge^2	3	10911.93	37.53
Ice + ice^2	3	10938.67	64.27
d_edge	2	10958.83	84.43
null	2	10983.12	108.72
ice	2	10983.28	108.88

were sampled from four whales. Sample sizes were insufficient to consider sex or age effects.

Neither the average dive duration, the distance dive depths were from the seafloor depth, the proportion of U-shaped dives, nor the proportion of V-shaped dives differed by ice period (Table 6). Average dive depth significantly varied by ice period ($p < 0.001$), with whales diving deeper prior to sea ice declines ($\overline{x} = 50.6$ m, 95% CI = 37.9–63.3 m) than after ($\overline{x} = 33.3$ m, 95% CI = 30.6–36.1 m). The proportion of square-shaped dives was also somewhat ($p = 0.06$) higher prior to the sea ice decline ($\overline{x} = 0.69$, 95% CI = 0.63–0.75) than after ($\overline{x} = 0.59$, 95% CI = 0.54–0.63).

There was no relationship between solar hour and dive depth before ice declines occurred. The smoothed function of solar hour was non-significant ($p = 0.12$), had a linear fit with no apparent cycle (Fig. 9, top), and explained almost no variation in the data (adjusted $R^2 = 0.007$). In contrast, solar hour was strongly significant after sea ice declined ($p < 0.001$) and suggested that the average dive depth of whales was deepest near solar noon ($\overline{x} = 38.9$ m; SE = 2.2) and shallowest near solar midnight ($\overline{x} = 24.5$ m; SE = 2.9). However, solar hour only explained approximately 5% of the variation in the data (adjusted $R^2 = 0.048$; Fig. 9, bottom).

3.4. Body condition index (BCI)

Between 1993 and 2016, BCI was measured for 47 yearling, 54 post-weaning, and 157 subadult whales harvested at Utqiaġvik. After 2017, BCI was measured for 10 yearling, 7 post-weaning, and 18 subadult whales. Yearling whales in the sample averaged 8.19 m (SD = 0.48) long with an average girth of 639.5 cm (SD = 61.0). Post-weaning whales averaged 8.34 m (SD = 0.43) long with an average girth of 587.9 cm (SD = 71.4). Subadult whales averaged 10.3 m (SD = 1.3) long with an average girth of 655.4 cm (SD = 76.8). BCI was also measured for 39 adult whales prior to 2017. However, no adult whales were sampled after the 2017 decline in sea ice as subsistence whalers have tended to harvest younger whales and not all whales were measured.

For yearlings, the best approximating model included the effect of season (spring versus autumn), but confidence limits for season include zero and $p = 0.12$. The next best approximating model (Δ AICc = 0.24) included no sources of variation in yearling body condition. The best model including ice period was 2.3 AICc units greater than the best approximating model and received no support; hence, there was no evidence that the BCI of yearlings changed after 2017 (Fig. 10).

For post-weaning whales, the best approximating model included an intercept ($\beta = 0.720$; $SE = 0.009$), an intercept adjustment for spring (β = -0.79; $SE = 0.019$), and an intercept adjustment for the post-2017 ice period (β = -0.083; $SE = 0.024$). The only other model within 2 AICc units included a negative trend; however, the confidence limits on the trend overlapped zero and $p = 0.3$. To put the BCI into terms of girth, the model suggests that a post-weaning whale of average length (834.7 cm) lost ~ 65.9 cm of girth overwinter prior to the decline in sea ice and then lost an additional 69.3 cm of girth overwinter after the decline in sea ice.

For subadult whales, the best approximating model included an intercept ($\beta = 0.644$; $SE = 0.003$), an intercept adjustment for spring (β = -0.051; $SE = 0.008$). Two models were within 2 AICc units of the best approximating model; both models included seasonal effects, however, one included ice periods and another included trend. The coefficients for ice period and trend both overlapped zero and $p > 0.3$. Hence, there was little evidence of an effect of ice period or trend, even though they were within 2 AICc of the best approximating model. To put the BCI into units of girth, the best approximating model suggests that a subadult whale of average length (1037.1 cm) loses ~53.1 cm of girth overwinter regardless of ice period.

3.5. Discussion

Both RSF and SSF results indicate bowhead movements during winter were strongly related to the distribution of sea ice. During January–March, there were virtually no locations (<0.01% of all locations) south of the ice edge. Whales not going south of the southern ice edge differs from their behavior in the summer and autumn in the

Table 4
Robust parameter estimates from the final RSF model of BCB bowhead whale winter habitat selection. Abbreviations of covariates: d_edge = distance to the southern ice margin in km; ice = sea ice concentration (%); V = seafloor current velocity (cm/s); gradT = denotes the gradient in temperature (°C/km); gradS = denotes the gradient in salinity (psu/km).

Parameter	Lower 95% CI	Estimate	Upper 95% CI	*p*-value
Intercept	−1.472	0.18	1.832	0.349
dist_edge	−0.0004	0.007	0.014	0.009
dist_edge^2	$-2.4{\cdot}10^{-5}$	$-1.3{\cdot}10^{-5}$	$-0.3{\cdot}10^{-5}$	<0.001
ice	0.625	1.008	1.391	<0.001
ice^2	−0.45	−0.317	−0.183	<0.001
V	0.011	0.044	0.077	0.019
gradT	0.062	0.28	0.49	0.013
gradS	−0.851	−0.571	−0.291	0.001

Table 3
Most parsimonious (lowest AIC) SSF model of BCB bowhead winter habitat selection. Abbreviations of covariates: d_edge = distance to the southern ice margin in km; ice = sea ice concentration (%); gradT = denotes the gradient in temperature (°C/km); step_km = step length in km. Step length is included to control for bias in parameter estimates (Forester et al., 2009).

Covariate	robust estimate	SE	Lower 95% CI	Lower 95% CI	*z*	*p*
dist_edge	0.008	0.005	0.019	−0.003	1.427	0.154
dist_edge^2	$-2.20{\cdot}10^{-5}$	$1.20{\cdot}10^{-5}$	$9.00{\cdot}10^{-7}$	$-4.50{\cdot}10^{-5}$	−1.879	0.06
ice	0.153	0.095	0.338	−0.032	1.618	0.106
ice^2	−0.133	0.02	−0.095	−0.171	−6.79	<0.001
gradT	0.075	0.034	0.142	0.008	2.2	0.028
step_km	−0.001	0.002	0.003	−0.006	−0.477	0.633

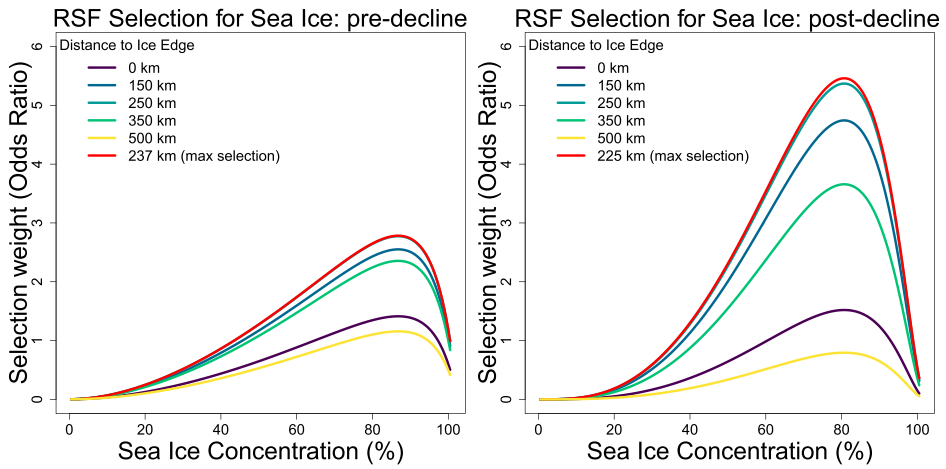

Fig. 7. Odds ratios of selection for sea ice concentration (%) across a range of distances from the southern ice margin (km) from the final RSF for BCB bowhead habitat selection prior to sea ice declines in 2017 (left) and after 2017 declines (right).

Beaufort and Chukchi seas, where habitat use is largely independent of sea ice. Staying north of the ice margin in winter may be related to their avoidance of killer whales, which are known to frequent the southern ice edge in winter (e.g., Lowry et al., 1987) but are relatively uncommon in BCB bowhead summer ranges. Killer whales are present in the Chukchi Sea between June and November and leave when sea ice forms (Melnikov and Zeh, 2007; Stafford, 2018). Approximately 8% of all bowhead whales harvested near Utqiaġvik (and >50% of whales >17 m) have tooth rake marks consistent with killer whale attacks (George et al., 2017; Breed, 2021). By analyzing photos collected during aerial surveys of the Chukchi and Beaufort seas, Willoughby et al. (2020) found that 18 of 33 (55%) bowhead carcasses had injuries consistent with killer whale predation, mostly in the Chukchi Sea. Killer whales are also known to affect the distribution of bowhead whales in the Eastern Canada-Western Greenland stock (Matthews et al., 2020; Breed, 2021).

Although the telemetry data suggest that most whales are staying north of the ice edge in winter, we know that our sample is not completely representative of the population because some bowhead whale calls were recorded on hydrophones south of the ice edge in 2018 and 2019 (C. Berchok, pers. comm.). Perhaps whales recorded south of the ice edge are larger whales which are less susceptible to killer whale predation (e.g., Breed 2021). The sample was dominated by immature whales (i.e., <13 m); 74% (20 of 27) prior to 2017 and 86% (6 of 7) after 2016. Using photogrammetry, Koski et al. (2006) estimated the length distribution of bowhead whales near Point Barrow, including calves. If we remove calves from their calculation, there should be approximately 60% immature whales. Hence, if mature whales are more likely to go south of the ice edge, our sample of mostly younger animals may not accurately represent how often bowhead whales generally range south of the ice edge, especially after the ice retreat.

We found no evidence that whales were avoiding warmer waters by remaining under sea ice or that the distribution of cold water was limiting. However, the hypothesis of Chambault et al. (2018), that bowhead whales may restrict their distribution to waters <2 °C due to thermoregulatory limits, was not testable because waters were typically colder than 2 °C across the study period and region. Furthermore, whales tended to use warmer waters prior to sea ice declines in 2017 (Fig. 4), because they were closer to the shelfbreak where deeper waters cool more slowly during winter and warmer waters may upwell.

Generally, winter movements were not as strongly tied to water masses as they are in autumn. Prior studies of autumn habitat selection indicated that whales followed cold, saline waters (<0 °C, 31.5–34.5 psu) of Pacific origin while on their "feeding migration" across the Chukchi Sea (e.g., Citta et al., 2018a, 2021). Although whales were predominantly found within a similar range of temperatures and salinities in this study (water mass #4 in Figs. 3–5), these waters are relatively common in the Bering Sea during winter, where they are actively forming under sea ice. Furthermore, although waters within this range of temperatures and salinities (i.e., <0 °C, 31.5–34.5 psu) are those we expect to have elevated densities of zooplankton in the Chukchi Sea during autumn, we do not expect krill to be limited to these waters in the Bering Sea during winter. Bowhead whales are also known to feed along strong salinity fronts in autumn, which often aggregate zooplankton (e.g., Moore et al., 1995), and are also thought to avoid areas dominated by relatively fresh river discharge, such as the Alaskan Coastal Water and Siberian Shelf Water, because these water masses contain reduced concentrations of larger zooplankton bowhead whales feed upon (Eisner et al., 2013; Ershova et al., 2015a, 2015b). The role of river discharge in determining bowhead distribution is reduced in winter due to freezing. For these reasons, we should not expect that bowhead winter movements in the Bering Sea would be as tightly linked to water mass as they are during autumn in the Chukchi Sea.

Although both SSF and RSF suggested bowhead whale movements were strongly influenced by the distribution of sea ice, there were some notable differences between the two approaches to examining selection. The RSF suggested that whales selected regions with higher concentrations of sea ice (~85%) than the SSF did (~65%) and selected regions that were on average farther from the ice edge (~250 km) than the SSF did (~150 km). These differences are likely attributable to the fundamental difference in temporal scale of inference of the two methods. RSFs are comparing where an animal is located, given what is available range-wide, while SSFs are measuring what an animal moves towards during its next movement, given its current location. The result consistent within both SSF and RSF analyses is that whales generally avoid areas with both the highest and lowest ice concentrations (Fig. 6).

Both the SSF and RSF also identified statistically significant positive selection for the gradient in bottom temperature (Tables 3 and 4). Whale locations co-occurred with areas with higher than average temperature gradients prior to sea ice declines (Fig. 8). These areas are associated with upwelling and advection in the central and western Bering Sea, especially where the Anadyr Current advects warmer basin waters northwards towards Anadyr Strait. In this same region, Citta et al. (2018a) used paired depth-temperature data from bowhead whales to infer that whales were diving into relatively warm Bering Shelf water that originated from south of the shelfbreak, where between December and March warmer water occurs at depth. In the central and eastern Bering Sea, areas with higher than average temperature gradients are also co-located with the seasonal ice edge. Because both the SSF and RSF detected selection for these areas, it is likely that temperature gradients help aggregate bowhead prey.

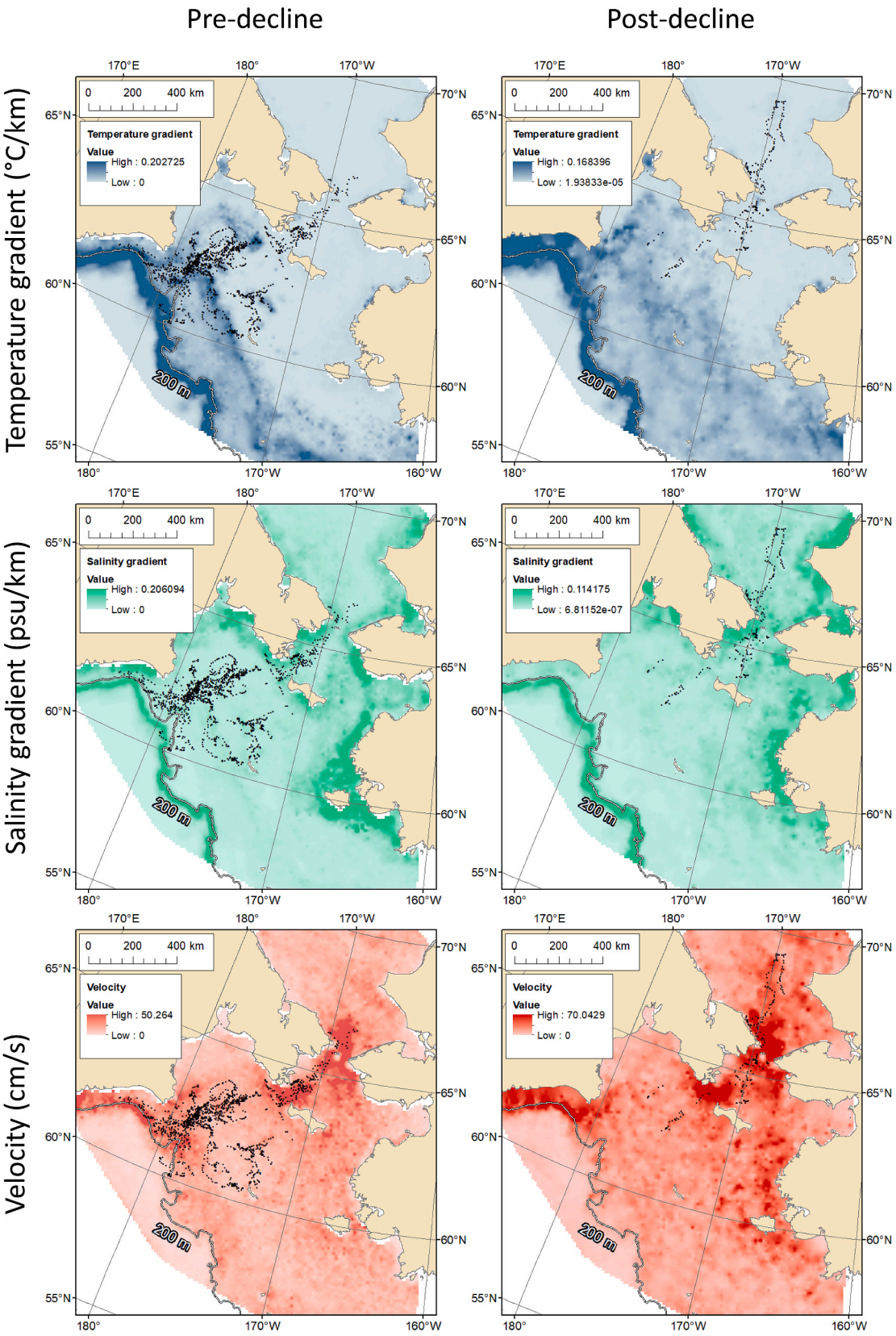

Fig. 8. Spatial distribution of the February averages of seafloor temperature gradient (°C/km), seafloor salinity gradient (psu/km), and seafloor velocity (cm/s) from RASM, prior to sea ice decline (left column) and after sea ice declines (right column). Bowhead whale positions are black dots. Higher gradients near the shelfbreak are partially an artifact of how the gradient was calculated and how RASM is structured. Cell size shifts below 200 m in RASM, resulting in artificially large gradients at the shelfbreak. Because of this, neither used nor available locations were considered in the habitat selection analyses for depth >200 m. Note elevated temperature gradients and current velocities in the western Bering Sea, from Cape Navarin, northwards towards Anadyr Strait. The month of February is provided as an example.

Table 5
Summaries of the 6-hr time-at-depth (TAD) histograms. Significance levels, period averages, and confidence levels are from linear mixed models where whales have random intercepts and temporally autocorrelated measurements. Hence, averages for each ice period account for differing sample sizes per whale and are not exactly equal to the average of rows. Average bathymetric depth is calculated at whale locations and target depth (i.e., most common dive depth) is calculated from the most visited depth bin for each 6-hr histogram period. Imm = immature, Mat = mature, M = male, F = female, and Unk = unknown.

Ice period	Row Labels	Age/sex	N	Average of bathymetric depth (m)	Proportion time at surface	Proportion time at seafloor	Target depth (m)
Pre-decline	B08-01	Imm/F	46	68.9	0.25	0.32	65.8
	B08-06	Imm/Unk	258	86.8	0.35	0.22	69.3
	B08-07	Imm/M	276	84.3	0.33	0.29	61.7
	B08-08	Imm/Unk	245	46.6	0.44	0.14	23.8
	B09-02	Mat/Unk	20	98.2	0.14	0.12	66.0
	B09-04	Imm/M	94	96.6	0.30	0.45	106.0
	B09-05	Imm/M	120	98.3	0.44	0.32	56.8
	B09-09	Mat/Unk	125	258.2	0.30	0.16	51.7
	B09-13	Imm/F	127	58.0	0.19	0.47	64.0
	B09-15	Imm/F	58	78.8	0.21	0.38	63.9
	B10-08	Imm/Unk	31	43.5	0.41	0.23	24.4
	B10-11	Imm/M	83	73.2	0.26	0.50	69.5
	B10-12	Imm/F	16	79.2	0.26	0.48	81.5
	B10-14	Imm/M	82	72.7	0.29	0.46	70.6
	B10-15	Imm/F	82	66.6	0.29	0.33	52.9
	B12-03	Mat/M	6	62.7	0.27	0.50	53.3
	B14-01	Imm/Unk	6	48.9	0.37	0.32	40.0
	B15-01	Mat/M	10	100.0	0.30	0.24	42.0
	mean			84.9	0.31	0.33	59.8
	95% CI			63.8–106.1	0.26 - 0.35	0.27 - 0.39	50.9–68.6
Post decline							
	B17-01	Imm/M	29	49.0	0.57	0.07	14.8
	B17-02	Imm/F	280	49.7	0.42	0.23	27.6
	B18-02	Imm/M	8	35.9	0.30	0.22	21.3
	B18-03	Imm/M	30	48.0	0.51	0.20	25.2
	B18-04	Mat/F	20	54.8	0.71	0.11	15.5
	mean			49.1	0.50	0.17	22.0
	95% CI			7.7–90.4	0.42 - 0.59	0.05 - 0.28	4.6–39.3
				p = 0.12	***p < 0.01***	***p = 0.02***	***p < 0.01***

The RSF detected more statistically significant covariates than the SSF did; in particular, the RSF detected statistically significant positive relationships with current velocity and a statistically significant negative relationship with salinity gradient. In the case of current velocity, this indicates that whales were co-located with areas of higher current velocity. Currents are generally higher in the western Bering Sea (e.g., Fig. 8) and are indicative of the main advective pathway for zooplankton. Currents may also create fronts and large-scale eddies that aggregate zooplankton, which are too fine-scale to be identified in the RASM data. Hence, it is not surprising that current velocity was not identified by the SSF as being significant.

We suspect that selection for low salinity gradients in the RSF model was spurious. In general, higher salinity gradients occur near-shore, in areas where there are either freshwater inputs or where new ice forms in polynyas, resulting in brine rejection. While we might expect salinity gradients to help aggregate zooplankton, whales did not use areas with elevated salinity gradients. Rather, we suspect that whales were simply using offshore areas which were also characterized by low salinity gradient (Fig. 8). Furthermore, large areas with low salinity gradients in the eastern Bering Sea were not used at all. The eastern Bering Sea is known to have lower concentrations of large zooplankton preferred by bowhead whales (e.g., Springer et al., 1996; Aydin et al., 2002). In general, covariates used in habitat selection models need to be interpreted with caution as they often serve as spatial proxies for productivity and zooplankton density, rather than representing the actual mechanisms by which zooplankton are aggregated. Indeed, wintering areas of bowhead whales, both in the Bering and southern Chukchi seas (Fig. 1), largely overlap the "Green Belt," an area of increased productivity that follows the shelfbreak in the northern Bering Sea and follows the Anadyr Current though the western Bering Sea to Bering Strait (see Fig. 2 in Springer et al., 1996).

After the 2017 decline in sea ice, whales frequented shallower water and shifted their time budget and the depths at which dives were focused away from the seafloor and towards the surface. No convincing patterns in dive behavior were detected by sex or age class. We did detect some differences in dive behavior by whales of unknown sex, namely whales of unknown sex had a lower than average probability of visiting the seafloor and shallower target depths. These patterns were driven by two different whales of unknown sex, B09–09 and B08-08 (Table 5). B09-09 was the only whale to venture south of the shelfbreak and had a lower than average probability of visiting the seafloor. B08-08 wintered north of St. Lawrence Island and targeted shallower depths than other whales prior to sea ice declines. In effect, this whale behaved much like other whales that wintered in Bering Strait.

Although no pattern of dive depth by time-of-day was detected prior to declines in sea ice, we did detect a highly statistically significant (yet highly variable) trend in dive depth with time-of-day after the 2017 decline in sea ice (Fig. 9). The pattern suggested that whales farther north dove shallower at night than during the day, which could be due to a variety of reasons. For example, this pattern might be expected if whales were shifting their diet towards krill (euphausiids), which are expected to exhibit DVM (Okkonen et al., 2020; Cohen et al., 2021), and away from copepods, which should be in diapause near the seafloor and not exhibiting DVM (Schmid et al., 2018). Studies have shown that krill

Table 6
Statistics from individually sampled dives. Significance levels, period averages, and confidence levels are from linear mixed models where whales have random intercepts and temporally autocorrelated measurements. Hence, averages for each ice period account for differing sample sizes per whale and are not exactly equal to the average of rows. Imm = immature, Mat = mature, M = male, F = female, and Unk = unknown.

Ice period	Whale ID	Age/sex	N	Average dive duration (min)	Average dive depth (m)	Distance of dive depth from seafloor (m)	Proportion square-shaped	Proportion U-shaped	Proportion V-shaped
Pre-decline	B12-03	Mat/M	55	16.3	−50.5	13.8	0.75	0.18	0.07
	B14-01	Imm/Unk	192	12.6	−37.8	7.8	0.68	0.25	0.07
	B15-01	Mat/M	158	12.2	−58.4	47.5	0.59	0.30	0.10
			Average	15.2	50.6	21.6	0.69	0.29	0.07
			95%CI	11.6–18.8	37.9–63.3	0–45.7	0.63 - 0.75	0.26 - 0.30	0.05 - 0.11
Post-decline	B17-01	Imm/M	269	13.3	−32.5	17.9	0.51	0.36	0.13
	B18-02	Imm/M	104	10.1	−26.5	10.7	0.63	0.32	0.05
	B18-03	Imm/M	602	11.1	−29.5	18.1	0.61	0.30	0.09
	B18-04	Mat/F	479	8.0	−33.3	23.3	0.60	0.28	0.12
			Average	12.5	33.3	15.6	0.59	0.30	0.10
			95%CI	9.7–15.2	30.6–36.1	11.4–19.7	0.54 - 0.63	0.27 - 0.32	0.08 - 0.13
				p = 0.26	***p < 0.01***	*0.60*	***p = 0.06***	*p = 0.14*	*p = 0.27*

exhibit DVM during the polar night, even in the high Arctic (Berge et al., 2009; Cohen et al., 2021), and most of the winter range of BCB bowhead whales is subarctic, suggesting there is sufficient light to trigger DVM. Perhaps when whales are feeding near the shelfbreak, their diet consists of a higher proportion of copepods that are upwelled onto the shelf, thereby masking DVM in bowhead dive behavior. When whales are farther from the shelfbreak, their diet may shift to include a higher proportion of krill, allowing patterns consistent with tracking DVM in krill to manifest in dive behavior. Alternatively, larger species of copepods may have simply been less available after 2017. Numerous studies indicate that the larger species of copepods, such as *Calanus glacialis/marshallae*, which are important prey for bowhead whales, are less abundant following warm periods (e.g., Eisner et al., 2014; Kimmel et al., 2018) and also following the 2017 decline in sea ice (e.g., Duffy-Anderson et al., 2019; Huntington et al., 2021; Kimura et al., 2022).

Indices of body condition did not change with sea ice declines for yearlings or subadult whales, but did decline for post-weaning whales (Fig. 10). The post-weaning age class is likely the most susceptible to environmental stress because they are newly weaned, thus inexperienced at feeding, and have shorter baleen which limits feeding efficiency. However, it is unclear if the shift in overwinter body condition is related to declining sea ice. Sample sizes are small after 2017, especially for the post-weaning age class. Second, the population has steadily increased in abundance since the 1980s (Givens et al., 2021) and may be approaching carrying capacity (*K*). Estimates of the BCB bowhead stock prior to commercial whaling indicate the stock numbered between ~10,000 and 23,000 (Woodby and Botkin, 1993; Brandon and Wade, 2006). The most recent estimates of abundance for this stock were made in 2019; an ice-base survey estimated 14,025 (CV = 0.228) whales (Givens et al., 2021) while an aerial survey estimated 17,175 (CV = 0.237) (Ferguson et al., 2022). Although estimates of historical abundance are highly uncertain, it is clear that the BCB bowhead whale stock is relatively abundant today and may be approaching (or exceeding) abundance prior to commercial whaling. We expect that body condition within juvenile age classes will be one of the first demographic parameters to be impacted by density dependence for long-lived mammals. A more thorough and updated analysis of body condition is warranted, especially since winter sea ice extent partially rebounded in the Bering Sea during 2020–2022.

3.5.1. Conclusions

Although some whales likely always wintered in the southern Chukchi Sea near Bering Strait, changing ice conditions will make overwintering at higher latitudes within the Chukchi Sea much more likely. Bowhead whales are thought to predominantly consume krill in the Chukchi Sea (Moore et al., 1995; Ashjian et al., 2010). Krill are not thought to reproduce as far north as the Chukchi Sea, rather they are advected into the Chuckchi through Bering Strait (Neibauer and Schell 1993; Siegel 2000, Berline et al., 2008). Climate warming has increased northward transport through Being Strait (Woodgate, 2018; Huntington et al., 2020), which has likely increased the northward advection of krill and other zooplankton from the Bering Sea into the Chukchi Sea. As such, increasing advection of bowhead prey into the Chukchi Sea, combined with lighter ice there, has likely made the Chukchi Sea a more favorable wintering ground. The Chukchi Sea has been an important feeding area in autumn, and we expect its importance as a feeding area in winter will increase as sea ice declines, flow through Bering Strait increases, and productivity within the Chukchi Sea increases.

We found little evidence suggesting bowhead whales are unable to cope with to the amount of environmental change that has occurred thus far. Maximum ice extent was more typical during 2020–2022 and the historical wintering areas of BCB bowheads have been mostly ice covered between January–March. Furthermore, post-weaning body condition in 2020 and 2021 returned to pre-decline levels (NSB unpublished data). However, we are not suggesting that the Bering Sea ecosystem has returned to pre-2017 conditions; sea ice continues to form later in winter and retreat earlier in spring and ecosystem-level effects may take time to manifest in the population parameters that are monitored, especially for such an extremely long-lived, slowly maturing species. To maintain harvest quotas established by the International Whaling Commission, BCB bowhead population parameters relating to health, body condition, and abundance are closely monitored (e.g., George et al., 2015; Stimmelmayr et al., 2018; Givens et al., 2013, 2021). Monitoring will need to continue in order to detect

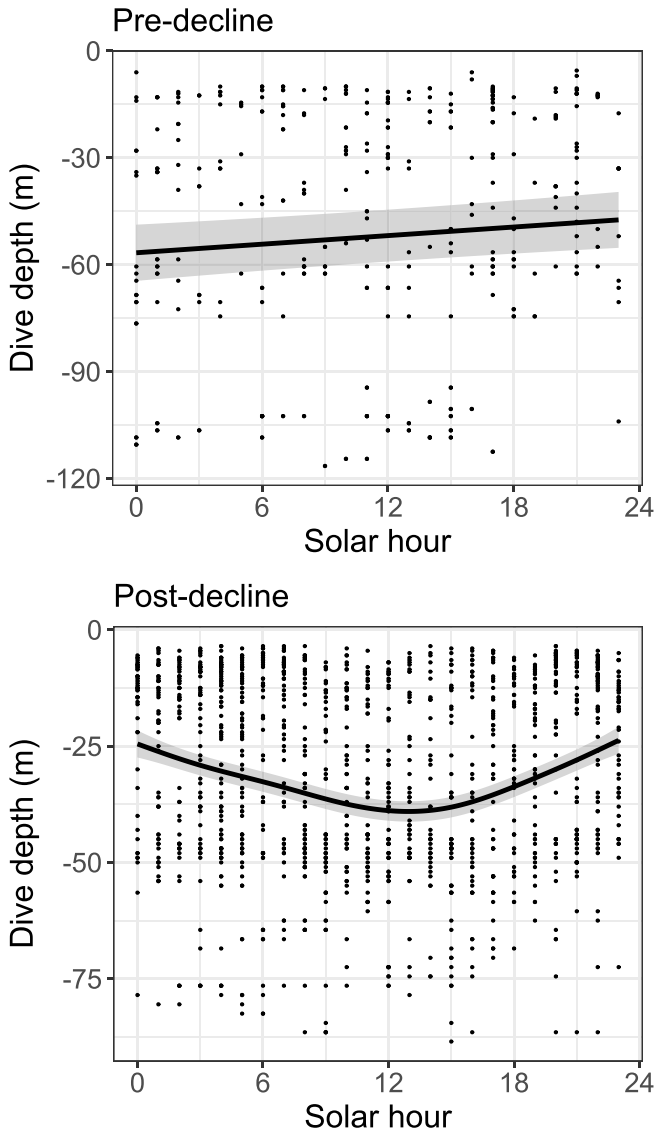

Fig. 9. Generalized additive model fits of dive depth, for dives ≥1 min that are square- or U-shaped, by solar hour. Whales were modeled as random intercepts with an autoregressive process of order 1 on a continuous time scale (i.e., corCAR1) using thin plate splines in R (Wood, 2003). Lines represent the smoothed fit and gray shading represents 95% confidence intervals for the fit.

population-level changes in the BCB bowhead whales if or when they occur.

Funding

This work was mainly supported by the U.S. Bureau of Ocean Energy Management (grant number M12PC00005) and the Office of Naval Research (grant number N00014-16-3019). Work in Canada was also funded by the Fisheries Joint Management Committee, Ecosystem Research Initiative, and Panel for Energy Research and Development.

Declaration of competing interest

The authors declare that they have no known competing financial interests or personal relationships that could have appeared to influence the work reported in this paper.

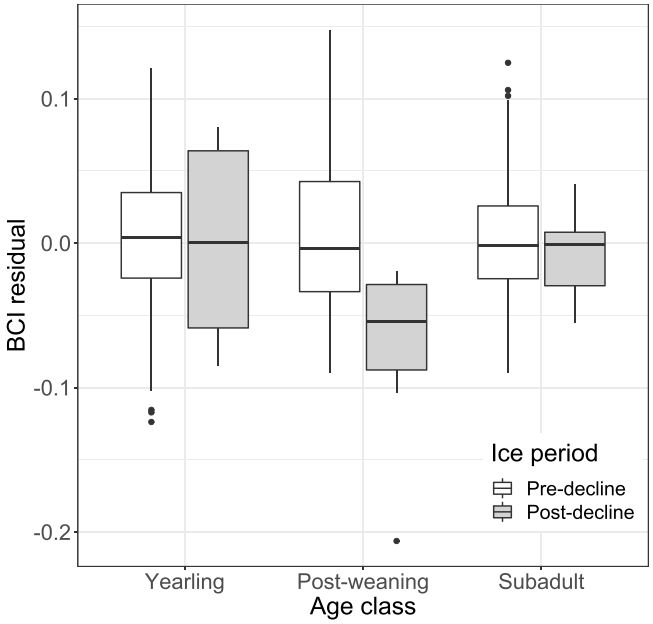

Fig. 10. Body Condition Index (BCI) residual by ice period and age class. Residuals are calculated after removing the effect of harvest season (spring or autumn). Boxes are bounded by the 25th and 75th percentile of the data, horizontal lines within boxes are medians, whiskers are 1.5 x interquartile range, and points are outliers.

Acknowledgements

This project involved contributions and hard work from many organizations, agencies, and individuals, including the following: Alaska Eskimo Whaling Commission, North Slope Borough Department of Wildlife Management, Barrow Whaling Captain's Association, and the Tuktoyaktuk and Aklavik Hunters and Trappers Committees, and the Department of Fisheries and Oceans Canada. Tagging expertise and support were provided by B. Adams, J. Aiken, P. Anashuak, H. Brower Jr., L. Brower, M. Donovan, J. Kippi, and C. Nyakik in Alaska, and D. Arey, L. Arey, C. Blakeston, R. Ettagiak, J. Felix Jr., M. Fleming, D.C. Gordon, L. Harwood, A. Jensen, P. Kasook, J. Keevik Sr., M. Kotokak, D. Leonard, K. Matari, A. Nichols, E. Raddi, G. Raddi, G. Raddi Jr., J Pokiak, C. Pokiak,S. Gruben Sr.,., D. Panaktalokin Canada. Bowhead whale research was conducted in the U.S. under a Marine Mammal Protection Act permits issued to NMFS (No. 782–1719) and the Alaska Department of Fish and Game (Nos. 14610 and 18890) and under Animal Care and Use permit Nos. 09–21, 2010–13R, 2012-020, 2013-20, 2014-03, 2015-25, 2016-23, 0027-2017-27, 0027-2018-29, 0027-2019-41. In Canada, research was conducted under Department of Fisheries and Oceans Scientific License Nos. S-07/08-4007-IN, S-08/09-4000-IN, S-09/10-4005-IN-A1, S-14/15-1027-NU, S-17/18-3034-YK and Animal Care Committee Nos. FWI-ACC-2007-2008-013, FWI-ACC-2008-031, FWI-ACC-2009-019, FWI-ACC-2010-034, FWI-ACC-2014-048, FWI-ACC-2017-35. RASM results used in the analyses were produced with support from the Department of Energy Regional and Global Model Analysis program, the Office of Naval Research Arctic and Global Prediction program, and the National Science Foundation Arctic System Science program. Computational resources for RASM were provided by the Department of Defense High Performance Computing Modernization Program.

References

Ashjian, C.J., Braund, S.R., Campbell, R.G., George, J.C., Kruse, J., Maslowski, W., et al., 2010. Climate variability, oceanography, bowhead whale distribution, and Inupiat subsistence whaling near Barrow, Alaska. Arctic 63, 179–194.

Avgar, T., Potts, J.R., Lewis, M.A., Boyce, M.S., 2015. Integrated step selection analysis: bridging the gap between resource selection and animal movement. Methods Ecol. Evol. 7 (5), 619–630.
Aydin, K.Y., Lapko, V.V., Radchenko, V.I., Livingston, P.A., 2002. A comparison of the eastern Bering and western Bering Sea shelf and slope ecosystems through the use of mass-balanced food web models. NOAA Technical Memorandum NMFS-AFSC-130. Available at: https://apps-afsc.fisheries.noaa.gov/Publications/AFSC-TM/NOAA-TM-AFSC-130.pdf.
Bates, D., Maechler, M., Bolker, B., Walker, S., 2015. lme4: linear mixed-effects models using Eigen and S4. R package version 1.1-8. http://CRAN.R-project.org/package=lme4.
Baumgartner, M.F., Mate, B.R., 2003. Summertime foraging ecology of North Atlantic right whales. Marine Ecology Research Series 264, 123–135.
Berline, L., Spitz, Y.H., Ashjian, C.J., Campbell, R.G., Maslowski, W., Moore, S.E., 2008. Euphausiid transport in the western Arctic Ocean. Mar. Ecol. Prog. Ser. 360, 163–178.
Bickham, J.W., Downing, H.K., Patton, J.C., George, J.C., Suydam, R.S., 2011. Molecular Assessment of Sex Chromosome Polymorphisms in the Bowhead Whale. Report to the International Whaling Commission Scientific Committee. SC/63/BRG14.
Braham, H.W., Fraker, M.A., Krogman, B.D., 1980. Spring migration of the western Arctic population of bowhead whales. US Natl. Mar. Fish. Serv. Mar. Fish. Rev. 42 (9–10), 36–46.
Brandon, J., Wade, P.R., 2006. Assessment of the Bering-Chukchi-Beaufort Seas stock of bowhead whales using Bayesian model averaging. J. Cetacean Res. Manag. 8 (3), 225–239.
Breed, G.A., 2021. Predators and the impacts of predation. In: Thewissen, J.G.M., George, J.C. (Eds.), The Bowhead Whale. Elsevier Publishing, ISBN 978-0-12-818969-6, pp. 457–470.
Breed, G.A., Cameron, M.F., VerHoef, J.M., Boveng, P.L., Whiting, A., Frost, K.J., 2018. Seasonal sea ice dynamics drive movement and migration of juvenile bearded seals *Erignathus barbatus*. Mar. Ecol. Prog. Ser. 600, 223–237.
Brueggeman, J.J., 1982. Early spring distribution of bowhead whales in the Bering Sea. J. Wildl. Manag. 46 (4), 1036–1044.
Burnham, K.P., Anderson, D.R., 2002. In: Model Selection and Inference: a Practical Information-Theoretic Approach, second ed. Springer-Verlag, New York, New York, USA.
Chambault, P., Albertsen, C.M., Patterson, T.A., Hansen, R.G., Tervo, O., Laidre, K.L., et al., 2018. Sea surface temperature predicts the movements of an Arctic cetacean: the bowhead whale. Sci. Rep. 8 (9658) https://doi.org/10.1038/s41598-018-27966-1. Available from:
Citta, J.J., Quakenbush, L.T., George, J.C., Small, R.J., Heide-Jørgensen, M.P., Brower, H., Adams, B., Brower, L., 2012. Winter movements of bowhead whales (*Balaena mysticetus*) in the Bering Sea. Arctic 65 (1), 13–34.
Citta, J.J., Quakenbush, L.T., Okkonen, S.R., Druckenmiller, M.L., Maslowski, W., Clement-Kinney, J., George, J.C., Brower, H., Small, R.J., Ashjian, C.J., Harwood, L. A., Heide-Jørgensen, M.P., 2015. Ecological characteristics of core areas used by western Arctic bowhead whales, 2006–2012. Prog. Oceanogr. 136, 201–222. https://doi.org/10.1016/j.pocean.2014.08.012.
Citta, J.J., Okkonen, S.R., Quakenbush, L.T., Maslowski, W., Osinski, R., George, J.C., Small, R.J., Brower, H., Heide-Jørgensen, M.P., 2018a. Oceanographic characteristics associated with bowhead whale movements in the Chukchi Sea in autumn. Deep Sea Research II 152, 121–131. https://doi.org/10.1016/j.dsr2.2017.03.009.
Citta, J.J., Lowry, L.L., Quakenbush, L.T., Kelly, B.P., et al., 2018b. A multi-species synthesis of satellite telemetry data in the Pacific Arctic (1987–2015): overlap of marine mammal distributions and core use areas. Deep Sea Research II 152, 132–153. https://doi.org/10.1016/j.dsr2.2018.02.006.
Citta, J.J., Quakenbush, L.T., George, J.C., 2021a. Distribution and behavior of Bering-Beaufort-Chukchi bowhead whales as inferred by telemetry. Pages 31–56. In: Thewissen, J.G.M., George, J.C. (Eds.), The Bowhead Whale. Elsevier Publishing, ISBN 978-0-12-818969-6.
Citta, J.J., Olnes, J., Okkonen, S.R., Quakenbush, L., George, J.C., Maslowski, W., Osinski, R., 2021b. Influence of oceanography on bowhead whale (*Balaena mysticetus*) foraging in the Chukchi Sea as inferred from animal-borne instrumentation. Continent. Shelf Res. https://doi.org/10.1016/j.csr.2021.104434.
Cohen, J.H., Last, K.S., Charpentier, C.L., Cottier, F., Daase, M., Hobbs, L., et al., 2021. Photophysiological cycles in Arctic krill are entrained by weak midday twilight during the Polar Night. PLoS Biol. 19 (10), e3001413 https://doi.org/10.1371/journal.pbio.3001413.
Comiso, J.C., Cavalieri, D.J., Markus, T., 2003. Sea ice concentration, ice temperature, and snow depth using AMSR-E data. IEEE Trans. Geosci. Rem. Sens. 41 (2), 243–252. Comiso, J.C., Cavalieri, D.J., Parkinson, C.L., P. Gloersen, P., 1997. Passive microwave algorithms for sea ice concentration: a comparison of two techniques. Remote Sens. Environ. 60, 357–384.
Danielson, S.L., Dobbins, E.L., Jakobsson, M., Johnson, M.A., Weingartner, T.J., Williams, W.J., Zarayskaya, Y., 2015. Sounding the northern seas. Eos 96. https://doi.org/10.1029/2015EO040975.
Duffy-Anderson, J.T., Stabeno, P., Andrews III, A.G., Cieciel, K., et al., 2019. Response of the northern Bering Sea and southeastern Bering Sea pelagic ecosystems following record-breaking low winter sea ice. Geophys. Res. Lett. 46, 9333–9842.
Duong, T., 2007. ks: kernel density estimation and kernel discriminant analysis for multivariate data in R. J. Stat. Software 21 (7), 1–16.
Duong, T., Hazelton, M.L., 2005. Cross-validation band-width matrices for multivariate kernel density estimation. Scand. J. Stat. 32 (3), 485–506.
Eisner, L., Hillgruber, N., Martinson, E., Maselko, J., 2013. Pelagic fish and zooplankton species assemblages in relation to water mass characteristics in the northern Bering and southeast Chukchi seas. Polar Biol. 36, 87–113.
Eisner, L.B., Napp, J.M., Mier, K.L., Pinchuk, A.I., Andrews III., A.G., 2014. Climate-mediated changes in zooplankton community structure for the eastern Bering Sea. Deep Sea Res. Part II Top. Stud. Oceanogr. 109, 157–171. https://doi.org/10.1016/j.dsr2.2014.03.004.
Ershova, E.A., Hopcroft, R.R., Kosobokova, K.N., Matsuno, K., Nelson, R.J., Yamaguchi, A., et al., 2015a. Long-term changes in summer zooplankton communities of the western Chukchi Sea, 1945–2012 Oceanography 28 (3), 100–115. https://doi.org/10.5670/oceanog.2015.60.
Ershova, E.A., Hopcroft, R.R., Kosobokova, K.N., 2015b. Inter-annual variability of summer mesozooplankton communities of the western Chukchi Sea: 2004–2012. Polar Biol. 38, 1461–1481.
Ferguson, M.C., Miller, D.L., Clarke, J.T., Brower, A.A., Willoughby, A.L., Rotrock, A.D., 2022. Spatial modeling, parameter uncertainty, and precision of density estimates from line transect surveys: a case study with Western Arctic bowhead whales. Report submitted to the Scientific Committee of the International Whaling Commission, SC/68D/ASI/01. Available at: www.iwc.com.
Fieberg, J., Matthiopoulos, J., Hebblewhite, M., Boyce, M.S., Frair, J.L., 2010. In: Correlation and Studies of Habitat Selection: Problem, Red Herring or Opportunity, vol. 365. Philosophical Transaction of the Royal Society Series B, pp. 2233–2244.
Forester, J.D., Im, H.K., Rathouz, P.J., 2009. Accounting for animal movement in estimation of resource selection functions: sampling and data analysis. Ecology 90, 3554–3565.
Fortin, D., Byeer, H.L., Boyce, M.S., Smith, D.W., Duschesne, T., Mao, J., 2005. Wolves influence elk movements: behavior shapes a trophic cascade in Yellowstone National Park. Ecology 86 (5), 1320–1330.
Fortune, S.M.E., Ferguson, S.H., Trites, A.W., LeBlanc, B., LeMay, V., Hudson, J.M., Baumgartner, M.F., 2020. Seasonal diving and foraging behaviour of Eastern Canada-West Greenland bowhead whales. Mar. Ecol. Prog. Ser. 643, 197–217. https://doi.org/10.3354/meps13356.
Fortune, S.M.E., Ferguson, S.H., Trites, A.W., Hudson, J.M., Baumgartner, M.F., 2021. Bowhead whales use two foraging strategies in response to fine-scale differences in zooplankton vertical distribution. Sci. Rep. 10, 20249 https://doi.org/10.1038/s41598-020-76071-9.
Freitas, C., 2012. argosfilter: Argos locations filter. R package version 0.63. https://CRAN.R-project.org/package=argosfilter.
Freitas, C., Lydersen, C., Fedak, M.A., Kovacs, K.M., 2008. A simple new algorithm to filter marine mammal Argos locations. Mar. Mamm. Sci. 24, 315–325.
George, J.C., Druckenmiller, M.L., Laidre, K.L., Suydam, R., Person, B., 2015. Bowhead whale body condition and links to summer sea ice and upwelling in the Beaufort Sea. Prog. Oceanogr. 136, 250–262.
George, J.C., Sheffield, G., Reed, D.J., Tudor, B., Stimmelmayr, R., Person, B.T., Sformo, T., Suydam, R., 2017. Frequency of injuries from line entanglements, killer whales, and ship strikes on Bering-Chukchi-Beaufort Seas bowhead whales. Arctic 70 (1), 37–46. https://doi.org/10.14430/arctic4631.
Givens, G.H., Edmondson, S.L., George, J.C., Suydam, R., Charif, R.A., Rahaman, A., Hawthorne, D., Tudor, B., DeLong, R.A., Clark, C.W., 2013. Estimate of 2011 abundance of the Bering-Chukchi-Beaufort Seas bowhead whale population. Report submitted to the Scientific Committee of the International Whaling Commission, SC/65a/BRG1. Available at: www.iwc.com.
Givens, G.H., George, J.C., Suydam, R., Tudor, B., Von Duyke, A., Person, B., Scheimreif, K., 2021. Correcting the 2019 survey abundance of Bering-Chukchi-Beaufort Seas bowhead whales for disturbance from powered skiffs. Report submitted to the Scientific Committee of the International Whaling Commission, SC/68C/ASI01. Available at: www.iwc.com.
Grebmeier, J.M., Cooper, L.W., Feder, H.W., Sirenko, B.I., 2006. Ecosystem dynamics of the pacific-influenced northern bering and Chukchi seas in the amerasian arctic. Prog. Oceanogr. 71, 331–361.
Harwood, L.A., Quakenbush, L.T., Small, R.J., George, J.C., Pokiak, J., Pokiak, C., et al., 2017. Movements and inferred foraging by bowhead whales in the Canadian Beaufort Sea during august and september, 2006–12. Arctic 70 (2), 161–176.
Heide-Jørgensen, M.P., Laidre, K.L., Nielsen, N.H., Hansen, R.G., Røstad, A., 2013. Winter and spring diving behavior of bowhead whales relative to prey. Animal Biotelemetry 1, 15.
Heinrichs, J.F., Cavalieri, D.J., Markus, T., 2006. Assessment of the AMSR-E sea ice concentration product at the ice edge using RADARSAT-1 and MODIS imagery. IEEE Trans. Geosci. Rem. Sens. 44 (11), 3070–3080.
Huntington, H.P., Danielson, S.L., Wiese, F.K., Boveng, P., et al., 2020. Is a dramatic transformation of the Pacific Arctic ecosystem underway? Nat. Clim. Change. https://doi.org/10.1038/s41558-020-0695-2.
Huntington, H.P., Sakakibara, C., Noongwook, G., Kanayurak, N., Skhauge, V., Zdor, E., Inutiq, S., Lyberth, B., 2021. Whale hunting in indigenous arctic cultures. In: Thewissen, J.G.M., George, J.C. (Eds.), The Bowhead Whale. Elsevier Publishing, ISBN 978-0-12-818969-6, pp. 501–517.
Johnson, D.S., London, J.M.. crawl: an R package for fitting continuous-time correlated random walk models to animal movement data. https://doi.org/10.5281/zenodo.596464.
Kimmel, D.G., Eisner, L., Wilson, M.T., Duffy-Anderson, J.T., 2018. Copepod dynamics across warm and cold periods in the eastern Bering Sea: implications for walleye pollock (*Gadus chalcogrammus*) and the Oscillating Control Hypothesis. Fish. Oceanogr. 27 (2), 143–158. https://doi.org/10.1111/fog.12241.
Kimura, F., Matsuno, K., Abe, Y., Ymaguchi, A., 2022. Effects of early sea-ice reduction on zooplankton and copepod population structure in the northern Bering Sea during

the summers of 2017 and 2018. Front. Mar. Sci. https://doi.org/10.3389/fmars.2022.808910.
Kinney, J.C., Assmann, K.M., Maslowski, W., Bjork, et al., 2022. On the circulation, water mass distribution, and nutrient concentrations of the western Chukchi Sea. Ocean Sci. 18, 29–49. https://doi.org/10.5194/os-18-29-2022.
Koski, W.R., Rugh, D.J., Punt, A.E., Zeh, J., 2006. An approach to minimize bias in estimation of the length-frequency distribution of bowhead whales (*Balaena mysticetus*) from aerial photogrammetric data. J. Cetacean Res. Manag. 8 (1), 45–54.
Laidre, K.L., Stern, H., Kovacs, K.M., Lowry, L., et al., 2015. Arctic marine mammal population status, sea ice habitat loss, and conservation recommendations for the 21st century. Conserv. Biol. 29, 724–737.
Ljungblad, D.K., 1986. Endangered whale aerial surveys in the Navarin basin and st. Matthew Hall planning areas, Alaska, 1986. In: Ljungblad, D.K., Moore, S.E., Clarke, J.T., Bennett, J.C. (Eds.), Aerial Surveys of Endangered Whales in the Northern Bering, Eastern Chukchi, and Alaskan Beaufort Seas, 1985: with a Seven-Year Review, 1979–85. Appendix E. MMS Technical Report 1111.
Lowry, L.F., Nelson, R.R., Frost, K.J., 1987. Observations of killer whales, *Orcinus orca*, in western Alaska: sightings, strandings, and predation on other marine mammals. Can. Field Nat. 101, 6–12.
Lubetkin, S.C., Zeh, J.E., Rosa, C., George, J.C., 2008. Age estimation for young bowhead whales (*Balaena mysticetus*) using annual baleen growth increments. Can. J. Zool. 86 (6), 525–538.
Lubetkin, S.C., Zeh, J.E., George, J.C., 2012. Statistical modeling of baleen and body length at age in bowhead whales (*Balaena mysticetus*). Can. J. Zool. 90, 915–931.
Manly, B.F., McDonald, L., Thomas, D.L., McDonald, T.L., Erickson, W.P., 2002. Resource Selection by Animals: Statistical Design and Analysis of Field Studies. Kluwer Academic Publishers, Dordrecht, Netherlands.
Maslowski, W., Clement-Kinney, J., Higgins, M., Roberts, A., 2012. The future of arctic sea ice. Annu. Rev. Earth Planet Sci. 40, 625–654.
Matthews, C.J.D., Breed, G.A., LeBlanc, B., Ferguson, S.H., 2020. Killer whale presence drives bowhead whale selection for sea ice in Arctic seascapes of fear. Proc. Natl. Acad. Sci. USA 117 (12), 6590–6598.
Melnikov, V.V., Zeh, J.E., 2007. Chukotka Peninsula counts and estimates of the number of migrating bowhead whales. J. Cetacean Res. Manag. 9, 29–35.
Moore, S.E., Laidre, K.L., 2006. Trends in sea ice cover within habitats used by bowhead whales in the western Arctic. Ecol. Appl. 16 (3), 932–944.
Moore, S.E., Reeves, R.R., 1993. Distribution and movement. In: Burns, J.J., Montague, J. J., Cowles, C.J. (Eds.), The Bowhead Whale. Society for Marine Mammalogy, Special Publication No. 2. Allen Press, Lawrence, Kansas, pp. 313–386.
Moore, S.E., George, J.C., Coyle, K.O., Weingartner, T.J., 1995. Bowhead whales along the chukotka coast in autumn. Arctic 48, 155–160.
Morin, P.A., Nestler, A., Rubio-Cisneros, N.T., Robertson, K.M., Mesnick, S.L., 2005. Interfamilial characterization of a region of the ZFX and ZFY genes facilitates sex determination in cetaceans and other mammals. Mol. Ecol. 14, 3275–3286.
Neibauer, H.J., Schell, D.M., 1993. Physical environment of the Bering Sea population. In: Burns, J.J., Montague, J.J., Cowles, C.J. (Eds.), The Bowhead Whale. Society for Marine Mammalogy, Special Publication No. 2. Allen Press, Lawrence, Kansas, pp. 23–44.
Okkonen, S., Ashjian, C., Campbell, R.G., Alatalo, P., 2020. Krill diel vertical migration: a diagnostic for variability of wind forcing over the Beaufort and Chukchi Seas. Prog. Oceanogr. 181, 102265.
Pease, C.M., 1980. Eastern bering Sea ice processes. Mon. Weather Rev. 108, 2015–2023.
Quakenbush, L.T., Citta, J.J., George, J.C., Small, R.J., Heide-Jørgensen, M.P., 2010. Fall and winter movements of bowhead whales (*Balaena mysticetus*) in the Chukchi Sea and within a potential petroleum development area. Arctic 63 (3), 289–307.
Quakenbush, L., Citta, J.J., George, J.C., et al., 2012. Seasonal movements of the Bering-Chukchi-Beaufort stock of bowhead whales: 2006–2011 satellite telemetry results. Report submitted to the Scientific Committee of the International Whaling Commission, SC/64/BRG1. Available from: www.iwc.int.
Pinheiro, J., Bates, D., R Core Team, 2022. nlme: Linear and Nonlinear Mixed Effects Models. R package version 3.1-158. https://CRAN.R-project.org/package=nlme.
Pinheiro, J., Bates, D., R Core Team, 2022. Nlme: linear and nonlinear mixed effects models. R package version 3.1-158. https://CRAN.R-project.org/package=nlme.
Schabenberger, O., Gotway, C.A., 2005. Statistical Methods for Spatial Data Analysis. Chapman Hall/CRC, Boca Raton, FL.
Siegel, V., 2000. Krill (Euphausiacea) demography and variability in abundance and distribution. Can. J. Fish. Aquat. Sci. 57 (3), 151–167.
Springer, A.M., McRoy, C.P., Flint, M.V., 1996. The Bering Sea Green Belt: shelf-edge processes and ecosystem production. Fish. Oceanogr. 5, 205–223.
Stabeno, P.J., Bell, S.W., 2019. Extreme conditions in the Bering Sea (2017–2018): record-breaking low sea-ice extent. Geophys. Res. Lett. 46, 8952–8959.
Stafford, K.M., 2018. Increasing detections of killer whales (*Orcinus orca*), in the Pacific Arctic. Mar. Mamm. Sci. 67, 696–706.
Stimmelmayr, R., George, J.C., Willoughby, A., Brower, A., Clarke, J., Ferguson, M., Sheffield, G., Stafford, K., VonDuyke, A., Sformo, T., Person, B., Sousa, L., Suydam, R., 2018. 2017 health report for the Bering-Chukchi-Beaufort Seas. Report to the Scientific Committee of the International Whaling Commission. SC/66B/AWMP/08. Available from: www.iwc.int.
Stroeve, J.C., Serreze, M.C., Holland, M.M., Kay, J.E., et al., 2012. The Arctic's rapidly shrinking sea ice cover: a research synthesis. Clim. Change 110, 1005–1027.
Therneau, T., 2022. A Package for Survival Analysis in R. R Package Version 3, 3-1.
Thurfjell, H., Ciuti, S., Boyce, M.S., 2014. Applications of step-selection functions in ecology and conservation. Movement Ecology 2, 4.
Venables, W.N., Ripley, B.D., 2002. Modern Applied Statistics with S, Fourth edition. Springer, New York. ISBN 0-387-95457-0. https://www.stats.ox.ac.uk/pub/MASS4/.
Vincent, C., McConnell, B.J., Ridoux, V., Fedak, M.A., 2002. Assessment of Argos location accuracy from satellite tags deployed on captive gray seals. Mar. Mamm. Sci. 18, 156–166.
Willoughby, A.L., Ferguson, M.C., Stimmelmayr, R., Clarke, J.T., Brower, A.A., 2020. Bowhead whale (*Balaena mysticetus*) and killer whale (*Orcinus orca*) co-occurrence in the U.S. Pacific Arctic, 2009–2018: evidence from bowhead whale carcasses. Polar Biol. 43 (11), 1669–1679. https://doi.org/10.1007/s00300-020-02734-y.
Wood, S.N., 2003. Thin-plate regression splines. J. Roy. Stat. Soc. 65 (1), 95–114.
Wood, S.N., 2011. Fast stable restricted maximum likelihood and marginal likelihood estimation of semiparametric generalized linear models. J. Roy. Stat. Soc. 73 (1), 3–36.
Woodby, D.A., Botkin, D.B., 1993. Stock sizes prior to commercial whaling. In: Burns, J. J., Montague, J.J., Cowles, C.J. (Eds.), The Bowhead Whale. Society for Marine Mammalogy, Special Publication No. 2. Allen Press, Lawrence, Kansas, pp. 387–407.
Woodgate, R.A., 2018. Increases in the Pacific inflow to the Arctic from 1990 to 2015, and insights into seasonal trends and driving mechanisms from year-round Bering Strait mooring data. Prog. Oceanogr. 160, 124–154.
Zeh, J.E., Clark, C.W., George, J.C., Withrow, D., Carroll, G.M., Koski, W.R., 1993. Current population size and dynamics. In: Burns, J.J., Montague, J.J., Cowles, C.J. (Eds.), The Bowhead Whale. Society for Marine Mammalogy, Special Publication No. 2. Allen Press, Lawrence, Kansas, pp. 409–489.